



Universidad
Carlos III de Madrid

BACHELOR THESIS

BIOMEDICAL ENGINEERING

Characterization of the effect of the substrate over functional and electrophysiological properties during culture of cardiomyocytes

Author: Lidia Gómez Cid

Tutor and director: Andreu Martínez Climent



Acknowledgements

This thesis has a special meaning to me, as it ends a very special period in my life. During all these years, I have had the luck of being surrounded by wonderful people who have known how to help and support me.

In the first place, I would like to thank my tutor Andreu M. Climent for his confidence in me and his patience. Also, for giving me an opportunity, providing motivation and valuing my work. I would like to thank Lucía Fuentes as well, who without knowing me, has offered me her help, attention and patience during the development of this thesis, and who in addition to a coworker has become a friend.

All the teachers that have helped us and encouraged us during this time also deserve a special mention, for all their time and for the eagerness they have shared with us.

Thanks to all my classmates and friends, for all the wonderful moments and their help. Special thanks to David and Eva for their support, and to Adrián for his help and all the fun times that have made this Bachelor Thesis a pleasant experience.

Thanks to all my family and especially to my parents and my sister, for their care and support to succeed in making my dreams come true and helping as much as possible. Finally, I would like to thank Carlos, a very special person, for all his patience and support in the hardest moments, his fine words and all his help that has encouraged me to continue and enjoy during all these years.

Thank you all for your company and support that have contributed enormously to make that period an unforgettable one.

Lidia Gómez, June 2015

Heart failure is a common, costly and potentially fatal condition commonly caused by cardiac cells depletion. Current therapies are aimed at protecting surviving cardiomyocytes, but they are unable to produce cardiac regeneration. Tissue engineered cardiac patches seem promising as cardiac repair tools, but they still pose many limitations as they do not mimic *in vivo* behavior. Recently, the use of flexible membranes for cardiac cell culture has been suggested as determinant in cardiomyocytic properties. The goal of this study is to compare for the first time key cardiomyocyte functional properties for cardiac repair such as proliferation, migration and displacement, and electrophysiological properties of HL-1 cardiac cell line in two different materials: (1) rigid Petri dishes and (2) flexible PDMS (polydimethylsiloxane) silicon wells. The study was carried out in the *Laboratorio de Órganos y Matrices Bioartificiales* belonging to the *Instituto de Investigación Sanitaria Gregorio Marañón*.

In order to assess these properties, HL-1 cells were cultured on both substrates and different tests were performed. Proliferation assay was carried out using alamarBlue® colorimetric test to calculate the percentage of reduction which is directly related to cell proliferation. Migration and displacement were determined by performing wound tests followed up using time-lapse imaging, and quantified using custom software made in Matlab. To study characteristic properties of cardiomyocytes, impulse propagation was recorded using optical mapping techniques, and results were analysed using custom software developed in Matlab to obtain conduction velocity information. At molecular level, expression of genes coding for proteins involved in impulse generation and propagation was analysed using qPCR (quantitative Polymerase Chain Reaction) technique.

Results show that HL-1 cells were able to grow and retain an adult cardiomyocyte phenotype on both substrates and spontaneous contractile activity was kept. In general, proliferation of HL-1 cells was confirmed to be very high, in opposite to migration and displacement. Proliferation was higher at early stages in Petri, but as the culture grew, proliferation rate got higher in silicon. Migration and displacement were quite low as wounds did not close within 60 hours, which is characteristic of adult cardiomyocytes. The results and observations suggest that these cells colonize new areas only by proliferation. Regarding the electrophysiological properties, conduction velocity showed to be higher in silicon wells (150 %). This result was supported by a higher expression of genes involved in action potential.

Results from this study support our hypothesis that the use of flexible membranes induces a more similar cardiac phenotype to that shown *in vivo*, especially characterized by higher conduction velocities. This opens new insights into cardiac patches, confirming that mechanical characteristics of the substrate play a role in cardiac cell phenotype. Silicon wells and other flexible membranes will allow further mimicking the *in vivo* environment by growing cardiac cells under mechanical and electrical stimulation.

Table of Contents

Acknowledgements	ii
Abstract	iv
Introduction	1
Objectives	2
Background	3
<i>Cardiomyocytes</i>	<i>3</i>
<i>Characterization techniques.....</i>	<i>9</i>
Proliferation test	9
Migration and displacement test	10
Optical mapping	11
Analysis of gene expression: PCR	17
Materials and Methods	19
<i>Cell culture.....</i>	<i>19</i>
<i>Proliferation assay.....</i>	<i>20</i>
<i>Migration and displacement test</i>	<i>22</i>
<i>Electrophysiological properties test</i>	<i>23</i>
<i>Analysis of gene expression.....</i>	<i>25</i>
Expenditure.....	27
Results	30
<i>Cell culture.....</i>	<i>30</i>
<i>Proliferation.....</i>	<i>31</i>
<i>Migration and displacement</i>	<i>33</i>
<i>Electrophysiological properties</i>	<i>35</i>
<i>Analysis of gene expression.....</i>	<i>36</i>
Discussion	39
<i>Main contributions.....</i>	<i>39</i>
<i>Comparison with previous studies.....</i>	<i>39</i>

<i>Clinical applications</i>	40
<i>Limitations</i>	40
<i>Future work</i>	41
Conclusions	42
Bibliography	43
Appendix	49
<i>Appendix 1: Migration and displacement software package</i>	49
<i>Appendix 2: Electrophysiology analyser software</i>	51
<i>Appendix 3: $2(-\Delta\Delta C(T))$</i>	52
List of tables and figures	53
<i>List of Tables</i>	53
<i>List of Figures</i>	53

Introduction

Cardiovascular diseases are the first leading cause of death worldwide [1], with more than 16 million deaths every year [2]. From these deaths, around 80% are caused by ischemic heart diseases or heart attacks [3]. Moreover, heart diseases cost the United States \$316.4 billion annually [4], so they are a large source of expenses [5]. In addition to that, people suffering from a myocardial infarction and surviving longer than a month have 11% probability of suffering a second episode [6]. Thus, it is of great importance to understand the mechanisms behind these diseases to design effective therapies.

The development of cardiac patches seems a promising way to treat patients after myocardial infarction [7]. After the infarction, some cardiac cells die due to the prolonged lack of oxygen supply. This tissue is usually repaired by fibroblasts interacting with cardiomyocytes, forming scar tissue. Myofibroblasts lack many electrophysiological properties and they are less polarized. However, they can partly depolarize myocytes in their vicinity, resulting in slower conduction than in healthy tissue. Moreover, these scars are heterogeneous because there are areas with greater numbers of surviving fibers. This results in asynchronous electric conduction that provokes a higher risk of future re-entries leading to ventricular arrhythmias [8].

Engineered patches may be a definite solution to solve this scar-tissue problem. Furthermore, they allow adequate simulation of cardiac tissue dynamics *in vitro* to obtain adequate models and to obtain more realistic responses of pharmacological agents and therapies, reducing the number of animals needed. Cardiac patches must have the potential to promote stem cell differentiation, cardiac regeneration and angiogenesis and they must have optimal structural, mechanical and electrophysiological properties [7]. Myocardial tissue has complex architecture and cell interconnections. To mimic the Extra Cellular Matrix (ECM) environment is one of the main challenges of tissue engineering, as it is crucial to obtain *in vivo* like phenotypes, such as higher conduction velocities and more efficient and synchronous contractions. Biodegradable scaffolds were often used, such as collagen, alginate and PGA (polyglycolic acid). New insights look into decellularized matrices, as they preserve natural structure [7].

The purpose of this work is to study and quantify the effect of using a flexible membrane as a substrate in different cardiomyocytic properties that play a key role in cardiac patches development in the *Laboratorio de Órganos y Matrices Bioartificiales* belonging to the *Instituto de Investigación Sanitaria Gregorio Marañón*. The proposed flexible membrane is silicon well made out of PDMS in contrast to conventional Petri dishes. Petri dishes are rigid and made out of polystyrene, which has a Young Modulus of 3-3.5 GPa [67]. PDMS (Polydimethylsiloxane) has a Young Modulus lower than 1MPa [9], which is much closer to that of the ECM (2.5-70kPa [10]). This flexibility does not only provide a more *in vivo*-like environment, but also offers the possibility of future studies about the impact of mechanical and electrical stimulation during cell culture, which may also contribute to the improvement of cardiomyocytic properties for cardiac patches.

Objectives

The main goal of this study is to test the effect of two substrates on different cardiomyocytic properties to evaluate their capacity for cardiac regeneration. The two substrates to be compared are (1) traditional Petri dishes used in cell culture and (2) silicon wells made out of PDMS. The hypothesis to be tested is whether if flexible membranes induce a cardiac phenotype more similar to that *in vivo* because of their similarity in mechanical properties with ECM. To achieve this, functional and molecular properties are to be explored. Functional properties include some general cell properties and some cardiomyocytic specific properties. The experiments are performed in HL-1 mouse cardiac cell line.

- Study general cell properties relevant for cardiac regeneration.
 - Compare proliferation of HL-1 cells in the two substrates.
 - Evaluate and observe differences in migration and displacement velocity in both substrates.
 - Record and compare how HL-1 cells close a wound area using time-lapse technique.
 - Design and implement a Guided User Interface to process the obtained images for migration and displacement velocity, and generate videos from the image sequences adding time code and spatial scale.
- Compare electrophysiological properties playing a role in cardiac function of HL-1 cells in both substrates.
 - Study and evaluate these specific properties at a functional level.
 - Check spontaneous impulse generation and contraction of cardiomyocytes in both substrates.
 - Obtain and study impulse propagation recordings through optical mapping techniques.
 - Design and implement a Guided User Interface to analyse the obtained recordings and obtain conduction velocity information and isochrone maps.
 - Contrast at the molecular level the expression of genes coding for proteins involved in electric impulse generation and propagation.

To achieve the purpose of this study (compare the effect of different substrate on cardiomyocytic properties), it is necessary to understand some basic concepts on the mechanisms and properties of cardiac cells and the characterization techniques that are going to be used. In this section, it is explained what cardiomyocytes are, what action potential is and the mechanisms behind it and its propagation, as well as the most common cardiac models used for *in vitro* experimentation. Also, the different characterization techniques in regard with the properties to be evaluated are introduced, such as proliferation assays, how to obtain migration and displacement information, optical mapping to assess electrophysiological properties, and gene expression analysis.

Cardiomyocytes

Cardiomyocytes are cells in which relay heart unique properties. Their main characteristic is their ability to transmit action potentials (electrical activity) and to contract as a result of it, thus, allowing the heart to contract synchronously and to pump blood. They are the most physically energetic cells in the body because of the continuous and coordinated contraction performed by the myofibrils that give it its striated form (**Fig. 1**). They also have intercalated discs forming unions between cells. These proteic unions offer very low electric resistance, allowing excellent electric conduction. There are different types of cardiomyocytes in the myocardium, depending on their location [11]. For this experiment, **HL-1** cells (an established cardiac murine cell line) were used because of its relative ease of use and its electrophysiological and contractile properties *in vitro* [12].

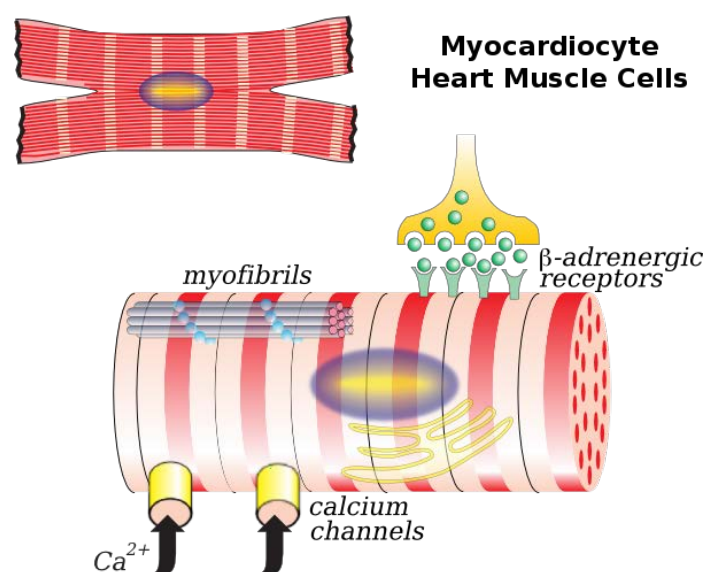


Fig. 1 Cardiomyocyte structure [13].

Action Potential and electric conduction

The action potential results from changes in the membrane potential of cardiac cells. This change is provoked by the inflow and outflow of ions across the membranes, and has four different phases: depolarization, plateau, repolarization and resting potential [14]. The major ionic currents playing a role in the action potential are sodium, calcium and potassium.

- **Sodium channels**

The inward sodium current is the main one exciting cardiomyocytes (I_{Na}). Sodium channels are usually closed during the resting potential and open when reaching a threshold causing an inflow of sodium ions that produce depolarization and so a raise in the membrane potential (phase 0). This is followed by the inactivation of sodium channels, which causes the cession of the sodium current (phase 1). These processes are crucial for the rapid conduction in the myocardium [14]. Sodium channels also coordinate contractions and maintain normal heartbeat. SCN5A is a gene from the sodium channels family (voltage gated). As a result, a higher expression of this gene is associated with a greater I_{Na} , and so, with a higher conduction velocity [15].

- **Calcium channels**

Calcium currents are also transient inward currents. They are activated by depolarization and inactivated later. They are responsible for long action potential durations (in comparison to other cell types) and for the plateau phase (phase 2) [14]. The longer this phase, the longer the effective refractory period (the period in which the cell cannot reactivate), which is essential to prevent cardiac arrhythmias and desynchronizations. CACNA1C is one of the main genes coding for a protein that forms up a subunit of calcium channels, and thus, its expression can be used as an indicator of calcium channels [16].

The process of excitation is linked to contraction because at the stage of the action potential in which calcium enters in the sarcolemma, it binds to actin and myosin triggering the contraction of the myofibrils. When cells contract, they reduce their volume, and when the cell relaxes, calcium leaves the sarcolemma recovering their original shape. How cardiac cells coordinate the electrical and the mechanical activity is key for the correct functioning of the cardiac tissue [17].

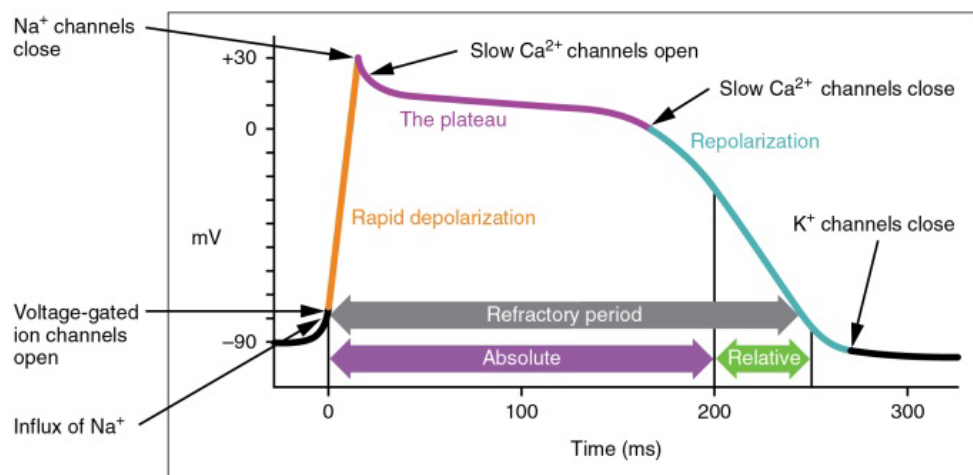
- **Potassium channels**

Potassium currents are outward and inward currents and are also termed delayed rectifier currents. They play a role in phase 2 because they produce an outward current that faces calcium inward current to maintain the plateau. They are also important in the repolarization phase in order to recover the membrane resting

potential (phase 3) and end the action potential. Potassium channels are the more diverse, and there are several potassium currents, each with individual roles [14]. KCNJ2 is a gene coding for potassium channels in the inward rectifying subfamily. In the cardiac tissue, these channels are responsible for restoring the membrane potential and for maintaining the refractory period [18].

The different phases of the action potential and the ions and currents playing a role can be observed in **Fig. 2**.

A



B

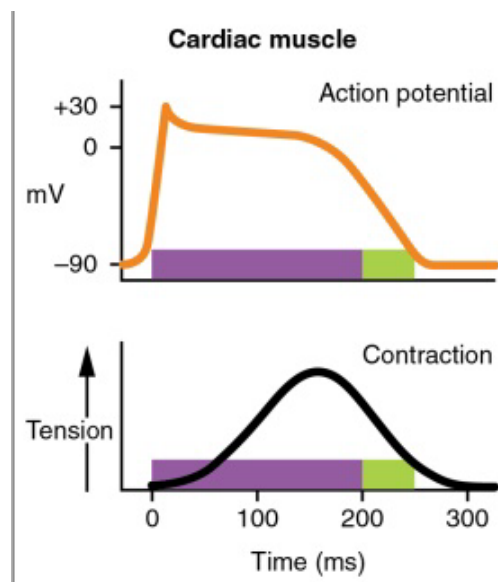


Fig. 2. Phases of the action potential (A) of a standard cardiomyocyte model and its relation with contraction (B) [19].

During phase 4, the cell keeps its resting membrane potential (no stimulation). In order to keep it, it is necessary to restore intracellular and extracellular sodium and potassium concentrations. Sodium-potassium pumps are crucial in this energy-requiring process that takes out of the cell sodium ions and into the cell potassium ions (**Fig. 3**)

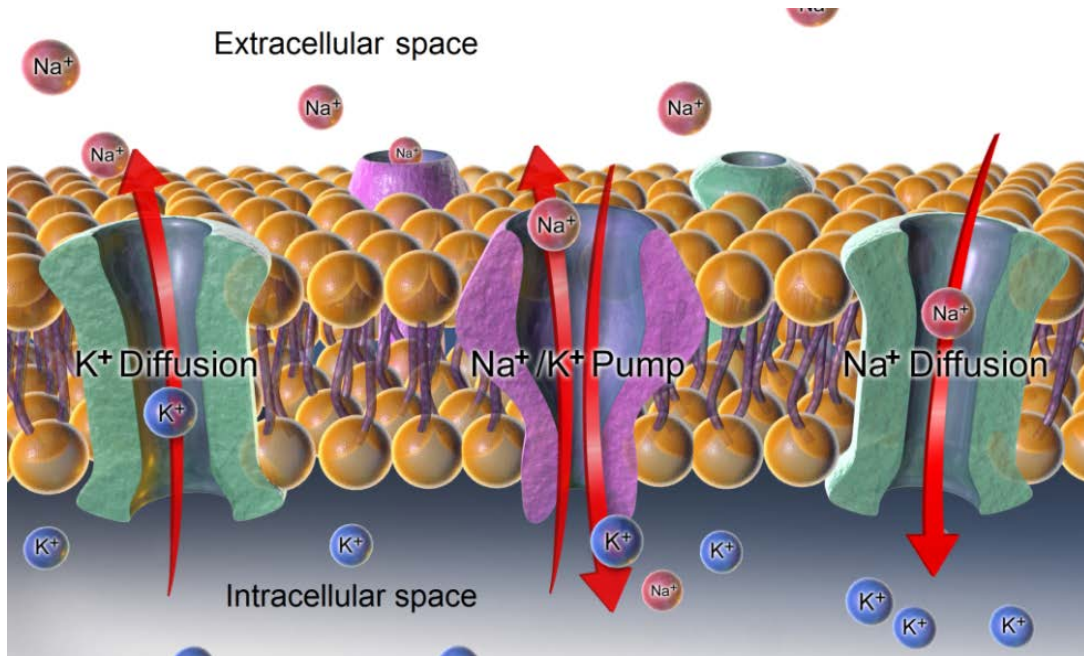


Fig. 3. Potassium channel, sodium-potassium active pump and sodium channel [20].

Although sodium, calcium and potassium channels are critical for the excitability of cardiac cells, to ensure effective and coordinated contraction, impulse transmission between cells is essential. This is achieved through gap junctions, which are located in the intercalated discs (membranes that separate two adjacent cardiomyocytes). They offer low resistance, favouring cell-to-cell communication. Gap junctions are very specialized protein structures that are made up of protein complexes named connexons. These connexons consist of different subunits (connexins) [14]. Connexin 43 is the major cardiac connexin and is mainly found in mammalian cardiac ventricles, which is encoded by gene GJA1 [21]. Connexin 40 (mainly expressed in the atria) and connexin 45 have also been identified in the heart. They are encoded by genes GJA5 [22] and GJA7 [23] respectively. Cardiac cell structure can be observed in **Fig. 4**.

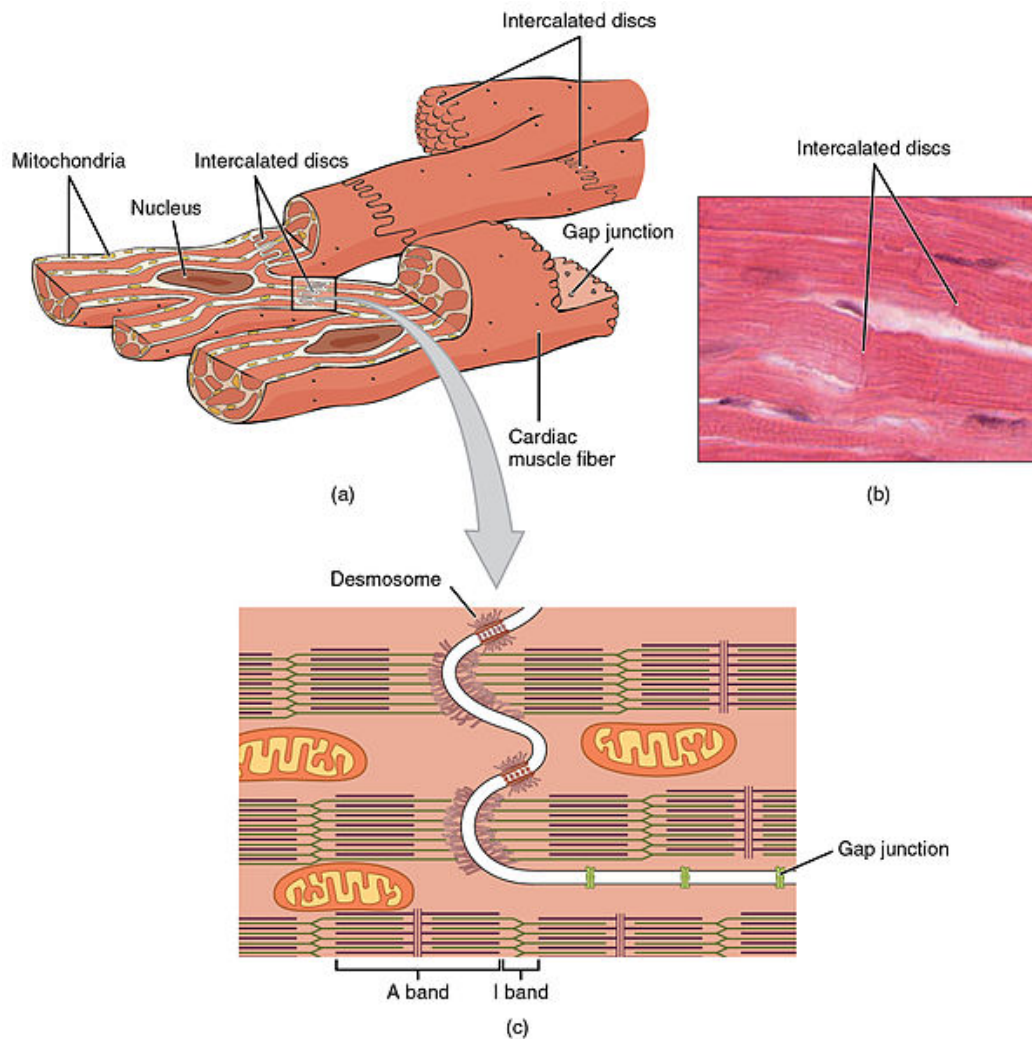


Fig. 4 Cardiac muscle structure [24].

Cardiac models

To study the effect of different substrates over the functional properties of cardiomyocytes, it is desirable to work with cells that resemble as much as possible adult human cardiac cells and that are stable, easy to grow and easy to work with *in vitro*. The three main types of models currently used in cardiovascular research are: primary cells, differentiated stem cells and cell lines.

- **Primary cells**

These are cells directly obtained from a biopsy of a human donor or from an animal used as model. Those obtained from adult tissue show similar properties to living tissue, but they lack the ability to form new intercellular connections and dividing capacity, because they are terminally differentiated. That is why they do not form monolayers. However, they can be used to analyse specific currents through patch-

clamp techniques [25]. Those obtained from neonatal animals (maximum 3 days after birth), are not yet terminally differentiated and may still form monolayers. Primary cells are in general difficult to keep. This, together with the fact that human healthy donors are scarce or that obtaining primary cells requires the use of living animals, limits their use considerably [26].

- **Differentiated from Stem Cells**

Cardiomyocytes can also be obtained after differentiation of pluripotent stem cells. Although there are several somatic stem cells that could be differentiated into cardiomyocytes, only two of them present acceptable efficiencies with actual protocols: Embryonic Stem Cells (ESCs) and induced Pluripotent Stem Cells (iPSCs).

ESCs can be obtained from embryos of human or animal origin. The main disadvantage is that they lack many adult cardiomyocyte characteristics, they soon stop dividing, and manipulation is difficult [27]. They may also pose ethical issues [28].

iPSCs are obtained from differentiated adult tissue by reprogramming the cell and taking it back to its embryonic like state. In that state, they are able to divide and the iPSCs can be forced to differentiate into different kinds of cells, allowing having on-demand number of desired cardiomyocytes [29]. They show very high conduction velocities and mimic better adult cardiomyocyte behavior ([30,31]). However, stabilizing an iPSC line, reprogramming and working with them requires experience, knowledge and time [32], and more important, current maturation protocols do not allow obtaining fully adult cardiomyocytes [33].

- **Cell lines**

They are a population of cells that has been established and that can undergo division for very long periods of time due to a mutation (immortalized). Because of that, they can be kept and passaged *in vitro* for prolonged periods keeping very similar properties. Moreover, working with them requires lower costs and they are easier to work with [34]. Nowadays, the only adult cardiac cell line capable of continuous division and spontaneous contraction is HL-1 [12], so that is why they are our choice to be used for the purpose of this study.

HL-1: It is a cardiac muscle immortal cell line that is able to retain cardiomyocytic properties over several passages (electrophysiological properties and contraction). They are derived from AT-1 cells, which come from an atrial tumor in a transgenic mouse. However, HL-1 cells can be serially passaged and recovered from frozen stocks in comparison with AT-1 cells. They have been demonstrated to serve as an experimental system to study cardiac function because of their gene expression, which is very similar to adult cardiac myocytes. Moreover, they have shown to be very similar to primary atrial cardiomyocytes with regard to electrophysiological properties. They are also well differentiated and highly proliferative (because of their

tumorous origin) which makes them very suitable for growing them *in vitro*. Because of all that, they represent a simple model to develop a better understanding of molecular and cellular regulation of cardiac function.

In order to maintain their phenotype and spontaneous contractile activity, they must be cultured under special media, including norepinephrine and retinoic acid [12]. This cellular model has shown to be very suitable for functional studies of cardiomyocytes, and especially for assessing cardiac ion channels response, which makes them very suitable for the purpose of this study.

Characterization techniques

Proliferation test

Proliferation is the increase in number of cells due to their subsequent division or reproduction (**Fig. 5**). In cardiomyocytes, it is an important property in myocardial development, but it occurs at a very low rate in adult cardiac cells [35]. However, it is a key property for cardiac regeneration. As the HL-1 cells used here are from tumorous origin, proliferation is a property that makes them suitable for its use *in vitro*, and thus, worth it to study.

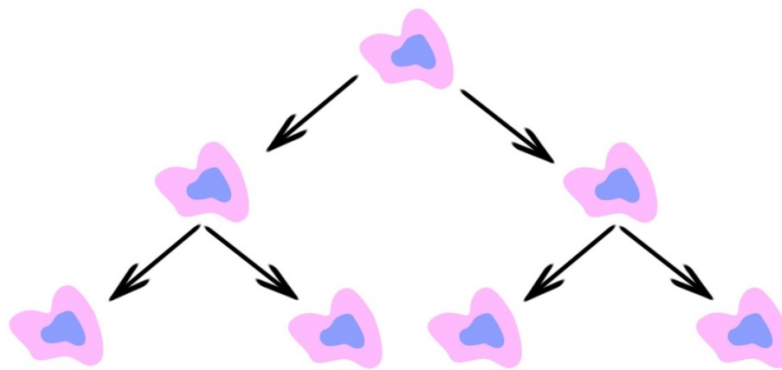


Fig. 5. Cell proliferation.

There are mainly three ways for assessing proliferation: measuring the rate at which DNA replicates, analysis of metabolic activity and recognition of surface antigens. For analyzing DNA synthesis, radioactive or labeled nucleotides are used. Using 3H-thymidine and BrdU (5-bromo-2'-deoxyuridine) are two of these methods [36]. In 3H-Thymine, the radiolabelled nucleotide incorporates into cells in the S phase (synthesis phase) of the cell cycle. This method is highly reproducible, but it requires specialized equipment and the use of radioisotopes [37]. BrdU is a thymine analog, and its use is non-radioactive. It incorporates into newly synthesized DNA substituting thymidine, thus labeling daughter cells. It can be detected by immunostaining with specific antibodies [38].

Other methods include antigen detection in proliferating cells through the use of antibodies, such as Ki-67, which recognises a protein expressed during proliferative phases of the cell cycle [39]. Other possible targets are topoisomerase IIB, phosphohistone H3 and PCNA [36]. Using bioluminescence-based detection of ATP has also been used to assess proliferation. Using the enzyme luciferase and its substrate luciferin, light is produced in presence of ATP [40].

Metabolic cell proliferation assays make use of changes in the medium produced by cell proliferation. Tetrazolium salts and alamarBlue® become reduced in an environment of active metabolic rate because of the activity of the enzyme lactate dehydrogenase during proliferation. This reduction produces a colorimetric change that can be measured with a spectrometer. These methods are cheaper and simpler with respect to the others, but are less reliable as they give an indirect measurement of proliferation [41]. The most used tetrazolium salt is MTT. Its main difference with alamarBlue® is that the second is soluble, non-toxic and more sensitive [42]. These properties allow making the whole study over the same sample, in contrast to other methods that require one different sample to obtain information at each time point. For all that, alamarBlue® will be the proliferation assay used for this study.

Migration and displacement test

Migration is the movement of cells in embryonic development, tissue repair or tumor invasion [43]. It plays a key role in cardiac repair in order to cover wounds and repopulate membranes effectively in future therapies in shorter periods of time [44]. The importance of migration and proliferation has been shown in zebra fish heart repair, but adult mammal cardiomyocytes seem unable to do so [45].

Time-lapse imaging is a technique that consists of taking images of a slow-changing object at a constant frequency. This frequency is less than the visual one, and when the frames obtained are played together at a faster speed, time seems to elapse and long events can be observed in a very short period of time.

This technique has been used to track cells in culture for days in order to assess proliferation, migration and displacement. Cells can be studied directly after seeding and observed while growing, or wound test can be performed. After making the wound, the cells are placed under the time-lapse and how they fill the wound space in time is observed. Time-lapse equipment to observe cells is especially prepared to be able to be introduced into incubators and with appropriate light to illuminate the cells.

Time-lapse images are very useful, as they allow having information of our system along time. These images can be further analysed with software in order to obtain information such as confluence in the wound area [43] and displacement velocity. Although there is some commercially available software, such as TimeLapseAnalyzer [46] and TLM-Tracker [47], each time-lapse equipment has specific image characteristics that may difficult feature segmentation and worsen the results in standard programs.

Optical mapping

Optical mapping is a technique used to obtain information about transmembrane potentials and calcium transients with high spatial and temporal resolution. It can be performed in monolayer cell cultures (*in vitro*) or in the whole heart (using a Langendorff system). It makes use of fluorescent dyes and of imaging systems to record this fluorescent signal that corresponds to calcium transients or electrical activity. Its main goal is to provide a better understanding of cardiac function.

Another common method to measure membrane potential is the use of intracellular recordings using glass pipette microelectrodes (patch-clamp technique). It consists of forming a seal between the cell membrane and the microelectrode and applying gentle suction (**Fig. 6**). The cell membrane can be broken and access to the cytoplasm is gained, so current recorded is the one flowing across all active channels (whole-cell patch-clamp). In perforated-patch technique, a pharmacological agent that creates channels in the portion of membrane patched is introduced in the pipette. Through these channels, access is gained to the interior of the cell and current is recorded. There are another patch-clamp modalities, such as cell-attached, cell-excised and outside-out patch clamp [48]. Although this technique provides absolute values for membrane voltage, and even for specific and individual channels, it is not possible to obtain simultaneous and stable recordings at multiple sites and it is highly invasive [49].

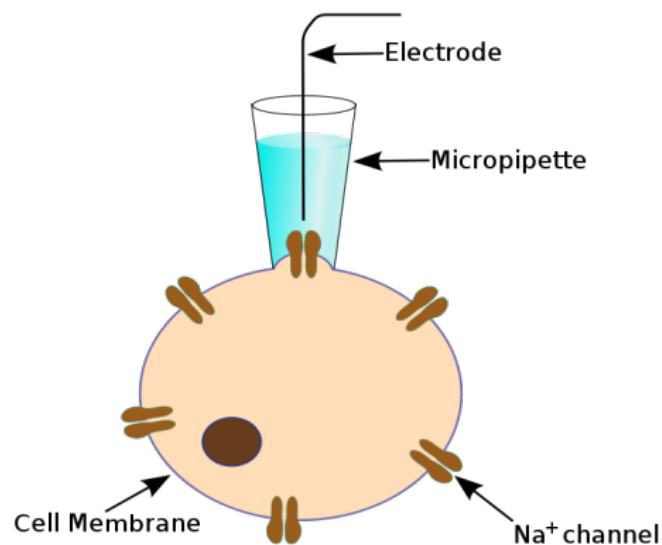


Fig. 6. Patch-clamp technique.

Optical recordings allow obtaining signal from a larger area and in a less invasive way for the cell, but they do not provide directly absolute information on intracellular calcium concentration and membrane potential [50]. However, both methods have shown similar results under different conditions (different frequency of stimulation, temperature, pharmacological agents,...) [51]. Another method that allows measuring electrical activity of several cells at a time is the use of surface electrodes. They can be patterned on the substrate

[52], and their main disadvantage is that they offer low spatial resolution, they provide information about extracellular potentials between two regions, they have low depth of field and interferences from electrical stimulation electrodes [53]. Their main advantages are that they provide absolute values of electric potential and are not invasive. Furthermore, electrograms have also shown to be in agreement with optical recordings [54], thus, making optical mapping a reliable technique which offers many benefits.

In order to carry out optical mapping recordings, a full system made out of light and detector sources, as well as filters and fluorescent dyes is needed [51] (**Fig. 7**).

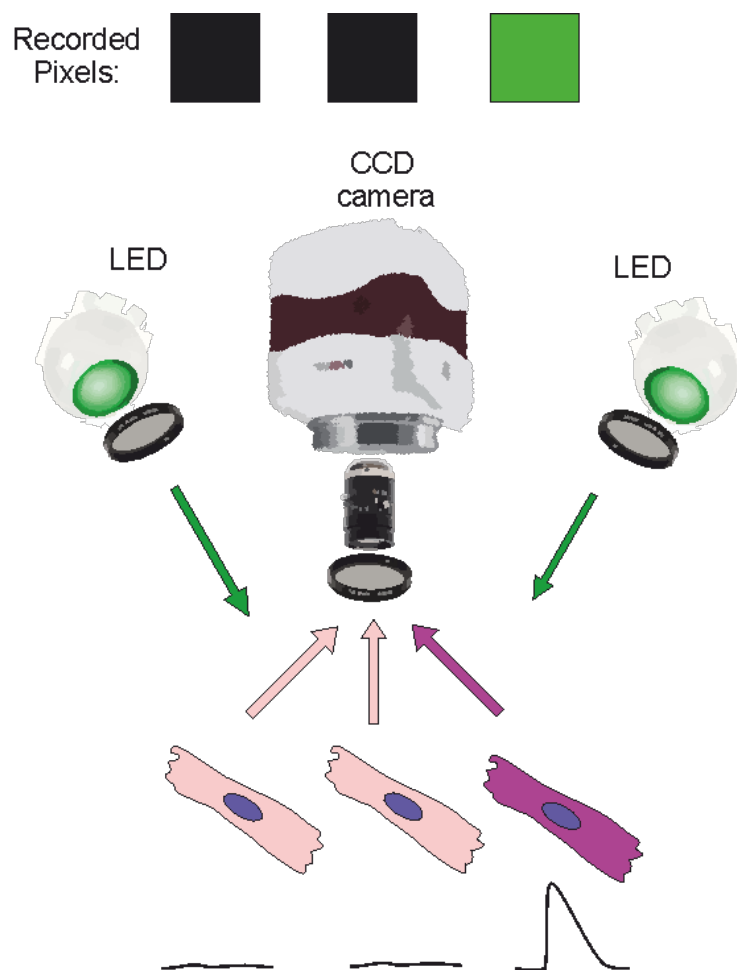


Fig. 7 Optical mapping system.

Optical mapping has shown huge clinical relevance, as it has allowed the study of electrophysiological mechanisms in monolayer cell cultures and in isolated hearts, such as propagation of electrical activity [55], action potential durations and calcium transients. It has also been used to visualize and study arrhythmias and to generate mathematical models of cellular electric activity [56]. An example of information obtained using optical mapping technique can be observed in **Fig. 8**.

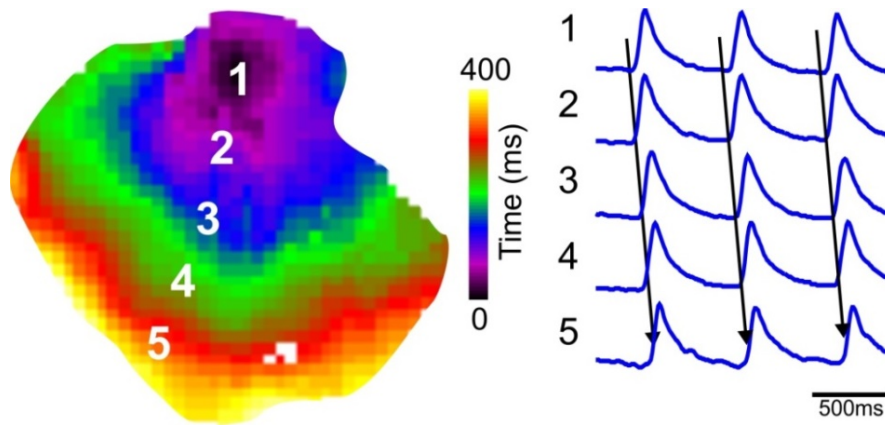


Fig. 8. Example of isochrone map and action potential signals obtained using optical mapping technique.

Fluorescent dyes

They are the source of signal in the optical mapping system. Thus, they may interact with the cell and change their radiation according to the feature to be observed. When fluorochemicals are excited with certain energy, they are able to absorb it and an electron from the ground state can be promoted into the excited state (electronic transition). Some of this energy is lost through non-radiative processes, and the electron relaxes back to the ground state emitting radiation of lower energy than the excitation one nanoseconds later [57] (**Fig. 9**). There are two main types of fluorescent dyes available for optical mapping: voltage-sensitive dyes and calcium indicators.

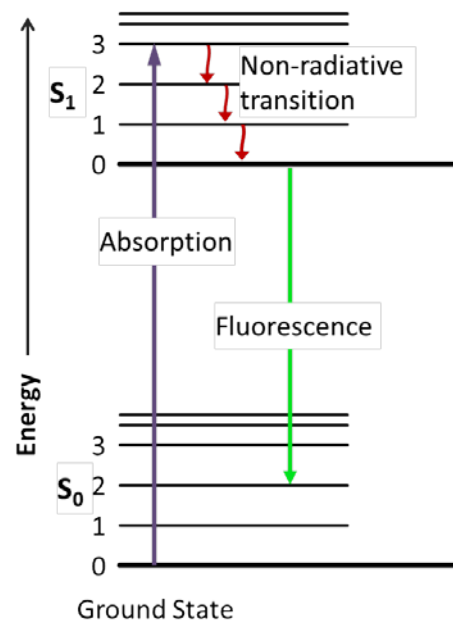


Fig. 9 Jablonski diagram of absorbance, non-radiative decay, and fluorescence [58].

- **Voltage-sensitive dyes**

Their working mechanisms can be explained by two theories. On the one hand, the electrochromic theory states that molecules undergo an electronic distribution during excitation, so energy of the electronic transition is altered [59]. On the other hand, the solvatochromic theory states that the electrical field reorients the dye molecules by the voltage gradient, producing changes in fluorescence [51].

Fast voltage-sensitive dyes are used in cardiac electrophysiology because their optical response occurs within microseconds. Styryl dyes have transmembrane location (**Fig. 10**). The hydrophilic groups anchor the molecule to the aqueous extracellular space and the hydrophobic end anchors within the bilipid layer of the membrane [59]. They are characterized too by large signal to noise ratio (SNR), short excitation wavelengths and large Stokes shift (to exclude scattered light, excitation light and background autofluorescence) [60].

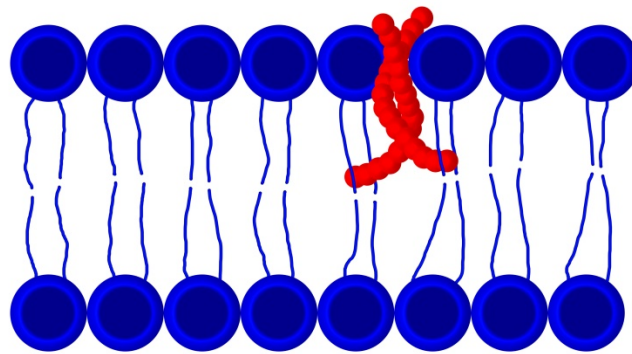


Fig. 10. Styryl dyes location in the cell membrane.

The most common dyes of this type are di-4-ANNEPS and di-8-ANNEPS. Both are rapidly internalized in the cell (they do not require long incubation times) and they are phototoxic, that is why they are better used for short-term experiments [61]. They respond to increases of membrane potential (hyperpolarization) and decrease fluorescent emission if excited at optimal wavelength [62].

- **Calcium indicators**

Calcium indicators respond to the binding of calcium ions by producing changes in fluorescence [63]. As calcium ions play a role in excitation-contraction coupling in the heart, calcium indicators are frequently used to study electrophysiological properties [51]. They contain lipophilic groups that allow their entrance into the cell, and once in the cell, they suffer a change in conformation due to an enzyme that allows calcium ions to bind. After the binding of the calcium ion, the fluorophore changes its quantum yield or suffers an excitation/emission shift [63].

The impact of the calcium dye in calcium dynamics of the cell must be minimized as much as possible. Cardiomyocytes show very large and rapid changes in calcium concentration, so a low-affinity and a fast-responsive dye is necessary [64]. Large-affinity dyes may prolong the calcium transient and lead to wrong interpretations [65]. Calcium indicators can be of two types: wavelength ratiometric and single wavelength non-ratiometric dyes [66]. Ratiometric measurements are obtained by taking the ratio between fluorescent intensity at two emission wavelengths. Absolute values of ions concentration can be obtained with appropriate calculations and calibrations using this type of dyes [50]. In single wavelength non-ratiometric dyes, collection at one emission wavelength is enough to determine relative calcium concentration (**Fig. 11**). They increase their fluorescence when it binds with calcium, and they only provide relative information on intracellular calcium [66].

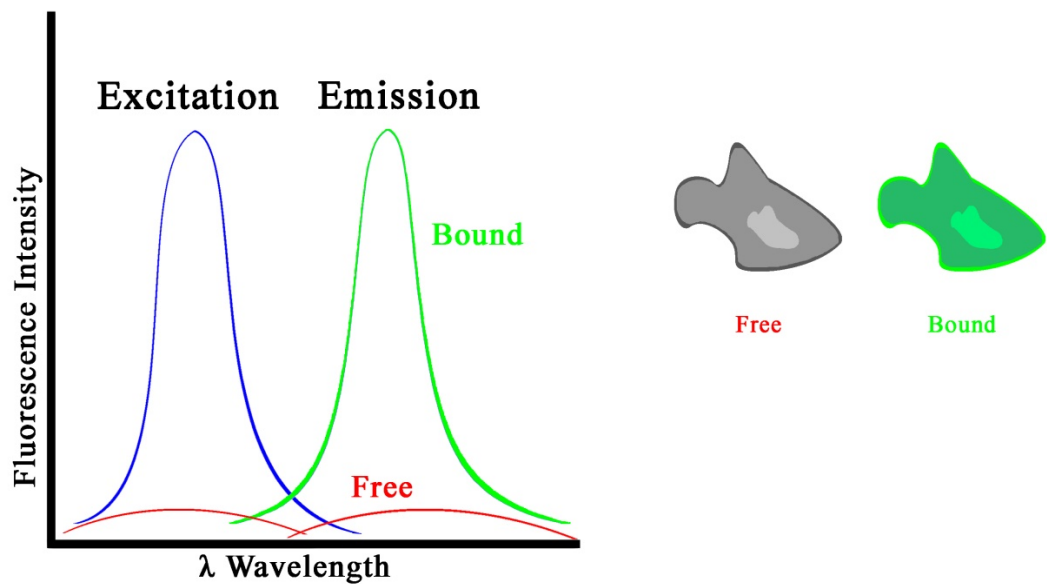


Fig. 11. Emission spectral shift in non-ratiometric calcium indicators.

Rhod-2 is a relatively low-affinity [67], single wavelength non-ratiometric dye and it is excited at 520 nm with a peak emission at 580nm [68]. It provides stable recordings and excellent SNR for long experiments (2 hours), as it is not phototoxic [69]. Although it may also accumulate in other organelles apart from the cytosol, it has been shown that this undesired loading is minimal [68].

Light Source

Proper illumination at the appropriate wavelength is essential for the correct excitation of the fluorophores. In cell monolayers, it is necessary to have stable and even illumination to obtain high SNR recordings [53].

Recently, Light-emitting diodes (LEDs) are commonly used for optical mapping purposes. In comparison to conventional white light sources and laser light, they have lower power consumption and fewer imaging artifacts [70]. They also offer narrow spectral output, lower costs [51], and are portable and flexible [71]. Their main concerns are cooling and sufficient output power. They can be controlled with a computer to allow complex and rapid wavelength switching (simultaneous calcium and voltage fluorescent signal recording) [72].

Larger emitted fluorescence results in larger signal, which can be achieved by more intense excitation. However, this may produce photobleaching of the fluorophores, so only enough excitation light must be used, and the dye must only be exposed when necessary (usually kept in the dark) [50].

Detectors

As electrical impulses in cardiac cells propagate fast and signal from the fluorescent dyes has low-strength (high background fluorescence), high-speed and low-noise photodetectors are needed. Two types of photodetectors are used to capture the fluorescent signal generated by the dyes: photodiode arrays and charged coupled device (CCD) cameras. They consist of two-dimensional arrays that transduce energy in the form of light into electrical energy [73].

Photodiodes have shown better results for moderate and high intensity light focused on a small spot, because noise decreases and the response is very fast. However, CCD video cameras offer very high spatial resolution [51]. Their pixel size is in the range of micrometers, and each frame integrates light over a discrete interval of time (exposure). Each frame corresponds to light collected simultaneously from all pixels [74]. Their main disadvantage is their slow frame rate, which can be improved by increasing pixel binning (reading several pixels at a time), but this decreases the resolution [49]. CCD cameras have shown to be very useful in the analysis of patterns of atrial arrhythmias [75].

EMCCDs (Electron Multiplying Charged Coupled Devices) are CCD derivatives which utilize impact ionization (avalanche process) to produce secondary electrons before conversion to electric signal. Because of that, they have larger SNR, more sensitivity, higher acquisition rates and better efficiency [76].

Filters

Filters are used in optical mapping to allow only selected wavelengths to pass through. Two types of filters are usually used, excitation filters and emission filters. Excitation filters are used to transmit only wavelengths near the excitation peak of the selected dye. This helps to reduce photobleaching. Emission filters are used to limit detection of the wavelength corresponding to the maximum emission peak of the fluorophore. They serve to increase SNR and obtain better quality images [51].

Analysis of gene expression: PCR

Cellular protein structures drive functional cell responses. In the case of electrophysiological properties, the presence of the three types of ion channels involved in the action potential (sodium, calcium and potassium) and the presence of connexins that form part of gap junctions are critical for correct electrical wave transmission among cells [14]. Thus it is of great importance to study cell behavior at the molecular level, as that leads to changes at the functional level.

In order to determine the amount of a specific protein in the cell, antibodies against it are generally used. There exist direct methods to detect them such as microscope imaging of immunostained proteins (using specific antibodies labeled with fluorescent molecules), immunoprecipitation, Western Blot, bicinchoninic acid assay (allows quantifying protein concentration), spectrophotometry and ELISA (Enzyme-Linked ImmunoSorbent Assay). However, antibodies are usually expensive [77].

Another method to estimate the amount of a certain protein is to use gene expression. By quantifying the amount of expression of the gene codifying for the protein of interest, the relative amount of protein present can be inferred. However, this relationship does not always hold, and as it is an indirect method (gene expression is being used as a marker of protein presence) it is not so reliable. It allows quantifying at the molecular level cell behavior and comparing samples. To quantify the amount of gene expression quantitative Polymerase Chain Reaction (qPCR) is the method commonly used.

PCR has radically transformed biological science as it is useful to diagnose diseases characterized by certain gene expression, and to carry out genetic tests in a very sensitive and fast manner [78]. To carry out a quantitative PCR, first, the genetic material has to be extracted from the sample. Then, the RNA (containing information on gene expression) is separated and extracted. As RNA is an unstable molecule (single stranded), a reverse-transcriptase protocol is carried out to obtain cDNA (double stranded). PCR is then performed normally [79].

This technique works by amplifying a specific DNA fragment by making copies out of it. It requires the presence of template DNA, nucleotides (the four bases that make up a DNA strand: A, T, C, G), DNA polymerase (the enzyme that links individual nucleotides together) and primers. Primers are DNA fragments that bind to a specific sequence (their complementary), thus indicating the place where amplification is to take place (indicating where the sequence corresponding to our gene of interest starts). They serve as the extension point for DNA polymerase to start adding nucleotides and so, to duplicate the strand [80].

In order to carry out the amplification process, these components are mixed together in a test tube or in 96-well plates and placed in a thermal cycler. The reaction occurs in three basic steps: first, the temperature is risen above the melting temperature of the two DNA strands in order for them to separate (denaturation) and be accessible for the primer and the DNA

polymerase. Then, the temperature is lowered to allow the primers to bind to its complementary sequence (hybridization or annealing). Finally, the temperature is risen again for the DNA polymerase to extend the primers by adding nucleotides and develop the DNA strand. With each cycle consisting of these three phases, the number of DNA copies doubles [81]. This process can be observed in **Fig. 12**.

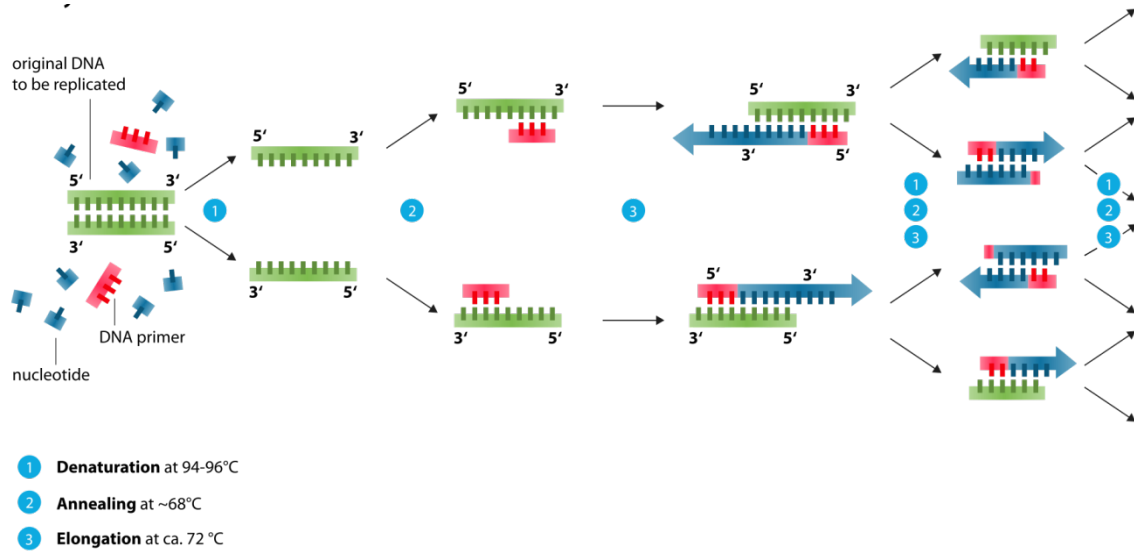


Fig. 12 Polymerase Chain reaction process [82].

When PCR is only used to detect the presence or absence of a specific DNA sequence, it is called qualitative. However, quantitative real-time PCR provides information on how much a sequence or a gene is present [83]. It needs the addition of a fluorescent dye that intercalates with double-stranded DNA to the mixture previously explained. In that way, by measuring the fluorescent intensity, it is possible to obtain relative information (by comparison within samples) on the number of copies, and so, on how much the gene is expressed [80].

Materials and Methods

In order to assess the impact of the different substrates, cells were grown and cultured following specific procedures in Petri dishes (p35) and first-use silicon wells. In this section, details on how the cells were cultured and how the different tests were performed are explained. Proliferation assay was carried out using alamarBlue® and migration and displacement by monitoring wound closing using time-lapse imaging. Electrophysiology was analysed by optical mapping and by quantifying the gene expression at the molecular level.

Cell culture

Cells were cultured on two different substrates: silicon wells and Petri dishes (p35) (**Fig. 13**).

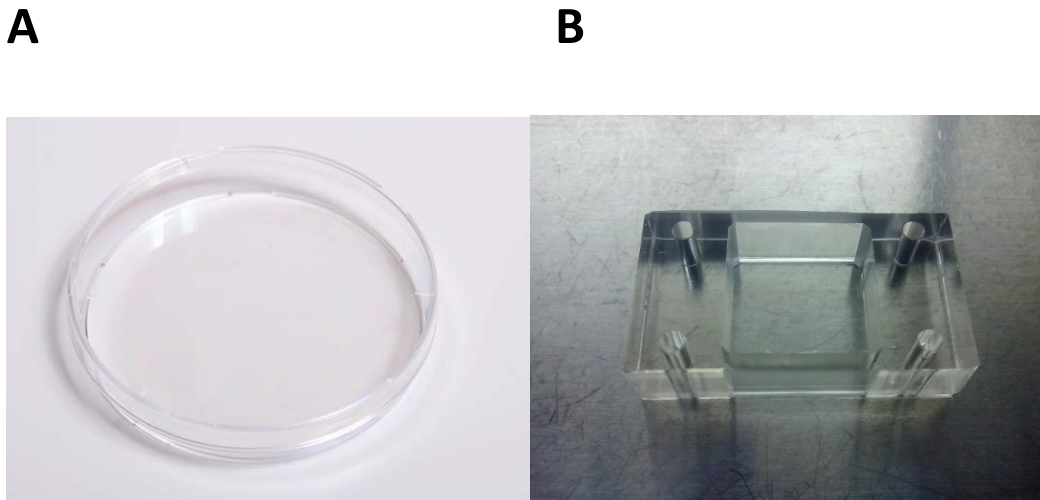


Fig. 13 Different substrates used: Petri dish (A) and PDMS silicon well (B).

HL-1 cells were seeded on both substrates after incubation of at least two hours with gelatin/fibronecting coating necessary for the cells to attach. After the incubation time, the coating was removed and the cells were seeded normally. HL-1 cells were cultured in Claycomb medium completed with 10% FBS (Fetal Bovine Serum), 1% PS (Penicillin/Streptomycin, 100 µg/ml final concentration), 1% L-Glutamine (2mM final concentration) and 1% Norepinephrine (0.1mM final concentration) to stimulate contraction. Media was changed periodically on Monday, Wednesday and Friday, and wrapped in aluminium foil, as it is light sensitive. Cells were grown at 37°C in an atmosphere of 5% CO₂ and 95 % air at a relative humidity of 95%.

When cells in flasks reached 100% confluence, they were passaged 1:2 using Soybean Trypsin Inhibitor incubated for 10 min. It was later inactivated by adding incomplete Claycomb

medium and centrifuged at 400xg for 10min. Cells were resuspended in complete Claycomb and counted using an improved Neubauer chamber.

Cells were initially recovered from frozen stocks (kept in 95% FBS and 5% DMSO gently added) at -180°C. Recovered cells were rapidly thawed in a 37°C water bath (2 min) and transferred into a centrifuge tube. They were centrifuged 10 min at 400xg and resuspended in completed Claycomb medium. Then, they were seeded normally. All these regular procedures for HL-1 culture were performed following standard HL-1 protocol [12], except for differences mentioned above.

Proliferation assay

AlamarBlue® is a commercial test that allows measuring quantitatively the proliferation of different cell lines. It is an oxidation-reduction indicator which is very simple to use, stable and not toxic. It works by detecting reduction of the medium resulting from cell metabolic activity. AlamarBlue® is uptaken by the cell, it is reduced by the removal of oxygen, which is proportional to the number of living cells, and this provokes a colorimetric change. Thus, we will find alamarBlue® after appropriate incubation conditions and time in two different forms: oxidized and reduced, each with a different maximum absorption peak. By measuring the absorbance at two different wavelengths, it is possible to know the concentration of both forms. Applying the appropriate formula (**Eq. 1**), it is determined the percentage of reduction of alamarBlue® (analogous to medium reduction and thus, an indicator of proliferation) [84].

$$\% \text{ Reduced} = \frac{(\epsilon_{OX})\lambda_2 A\lambda_1 - (\epsilon_{OX})\lambda_1 A\lambda_2}{(\epsilon_{RED})\lambda_2 A'\lambda_2 - (\epsilon_{RED})\lambda_2 A'\lambda_2}$$

Eq. 1.

Where,

ϵ_{OX} = molar extinction coefficient of alamarBlue® oxidized form (Blue)

ϵ_{RED} = molar extinction coefficient of alamarBlue® reduced form (Red)

$A\lambda$ = absorbance at each of the different wavelengths for the test well

$A'\lambda$ = absorbance at each of the wavelengths for the control well (without cells)

λ_1 = 570 nm (maximum absorption peak of reduced alamarBlue®)

λ_2 = 600 nm (maximum absorption peak of oxidized alamarBlue®)

In order to perform this proliferation assay, HL-1 cells were seeded in three p35s and three silicon wells at three different initial concentrations (**Table 1**). Cells were seeded on day 1 and cultured with 208µL of medium/cm². From day 2 to day 5, equal amount of media were changed at 5pm and left overnight (to be reduced because of cell proliferation). In the

following morning after incubation (from day 3 to day 6), alamarBlue® was added at 9 am in a concentration of 1 $\mu\text{L}/10 \mu\text{L}$ of medium and left in the incubator for 4 hours. After this time, 300 μL of each sample (medium + alamarBlue®) were loaded into 96-well plates (100 $\mu\text{L}/\text{well}$, 3 replicates). Absorbance for each well was measured using EMax® Plus Microplate Reader from bioNova cientifica. With this absorbance values at two different wavelengths, the formula to obtain the % of reduction in the medium was used (**Eq. 1**). The process can be observed in **Fig. 14**.

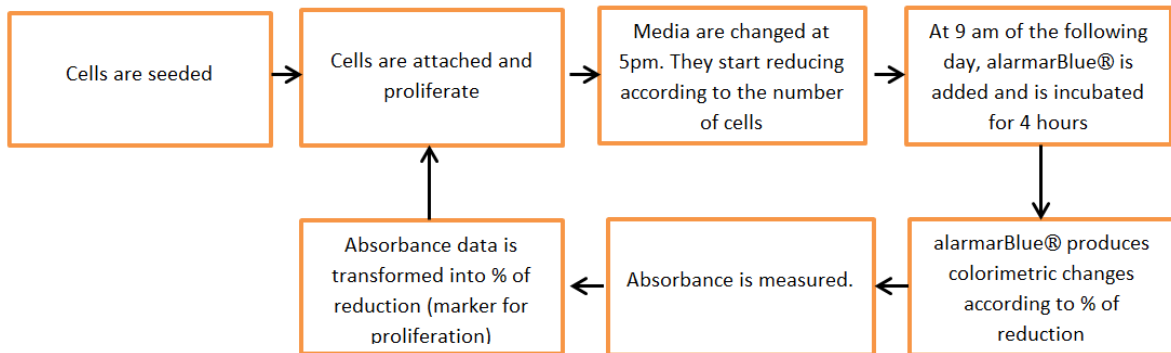


Fig. 14 Proliferation assay steps.

Substrate	Area	Medium quantity added (208 $\mu\text{L}/\text{cm}^2$)	alamarBlue® quantity added (1 $\mu\text{L}/10 \mu\text{L}$ medium)	Initial cell concentration
Silicon	4 cm^2	830 μL	83 μL	17500 cells/ cm^2 (+)
				35000 cells/ cm^2 (~)
				75000 cells/ cm^2 (-)
p35 (Petri dish)	8 cm^2	1660 μL	166 μL	17500 cells/ cm^2 (+)
				35000 cells/ cm^2 (~)
				75000 cells/ cm^2 (-)

Table 1. Proliferation test.

Migration and displacement test

To assess migration and displacement in both substrates, three p35s (Petri dishes) and three silicon wells of PDMS were used. In order to generate the wound, full confluence must be achieved (cells must be covering the whole substrate). One method to generate the wound consists in placing a stencil attached to the substrate and taking it out after the cells have covered all the surrounding area (**Fig. 15**). The wound is the area where the stencil was initially placed, as it was not covered by cells. This method does not damage the cells at the interface, but induces larger wounds due to the stencil area. One wound test in each substrate was carried out with this method. Another method is generating the wound scratching with the tip of a pipette (a straight line). This method may damage cells at the interface, and wound area cannot be controlled. However, it generates narrower wounds. The other two samples of each material were performed with this test.



Fig. 15. Stencil for wound generation.

After wound induction, how cells migrate and displace to close the injury was recorded using time-lapse equipment (Lumascope 400 iVue, etaluma, **Fig. 16**) inside the incubator for 60 hours. This equipment was configured to take an image of the wound area every five minutes.



Fig. 16. Lumascope 400 iVue Time-lapse.

To process those images, custom software in MATLAB (The MathWorks) was developed. This software is a Guided User Interface that allows loading the image sequences, choosing the wound area and intensity thresholds (semiautomatic method). It provides the user with a graph of confluence over time obtained from analysing the images sequentially by segmenting the cells using intensity thresholding and morphological operators. It also gives the possibility of creating a video from the sequence introduced, and adding a bar with the space scale according to the objective of the lens used and time codes.

Electrophysiological properties test

To study the electrophysiological properties of HL-1 cells after growing in both substrates, cells were seeded and grown normally. Four samples confirming electric impulse propagation of each substrate were employed to assess these properties. After reaching full confluence, spontaneous contractile activity of the cardiomyocytes was checked under the microscope. In order to proceed with the optical mapping technique, two fluorescent dyes were initially used: di-8-ANNEPS (voltage dye) and rhod-2 (calcium indicator).

Rhod-2 needs to be incubated for at least 30 min to be properly uptaken by the cell. Thus, a solution of 3ml of Tyrode solution, 16 μ L of Probenecid and 10 μ L of rhod-2 was prepared and added into the wells to be mapped. To map with di-8-ANNEPS 35 μ L of dye are added to 3mL of Tyrode. After 30 min in the incubator in the case of rhod-2 and 10 in the case of di-8-ANNEPS, the culture was washed and electrical activity and cell viability was confirmed with the optical mapping system. Working with di-8-ANNEPS did not show very good results as cells seemed to die early. Thus, from now on, only experiments performed with rhod-2 will be shown.

In order to excite rhod-2, cell cultures were illuminated with two filtered green LED light source (CBT-90-G, peak output 58W, peak wavelength 524nm; Luminus Devices, Billerica, USA), with a plano-convex lens (LA1951; focal length=25.4mm, Thorlabs, New Jersey, USA). The green excitation filter used was D540/25X (Chroma Technology, Bellows Falls, USA). Fluorescent emitted was recorded using an EMCCD camera (Evolve-128: 128x128, 24x24 μ m-square pixels, 16 bit; Photometrics, Tucson, AZ, USA), with a custom emission filter (ET585/50-800/200M; Chroma Technology) in front of a high-speed camera lens (DO-2595; Navitar Inc., Rochester, USA). The system can be observed in **Fig. 17**.

Once electrical activity was confirmed, lines were made in the cell culture by scratching in order to kill cells and only allow electric conduction to happen in a certain direction. This simplifies the electric activity and eases future measurements. Moreover, cells were stimulated with two electrodes placed as shown in **Fig. 18** in order to record synchronized signals from a wide range of regions in the wells.

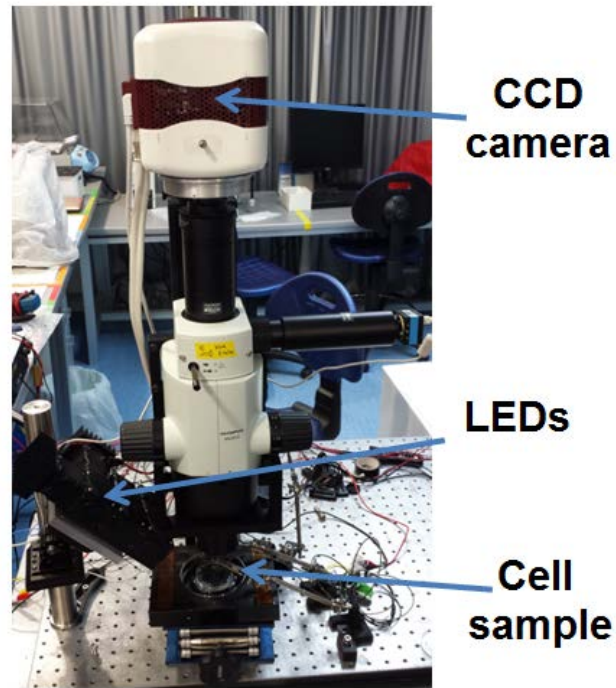
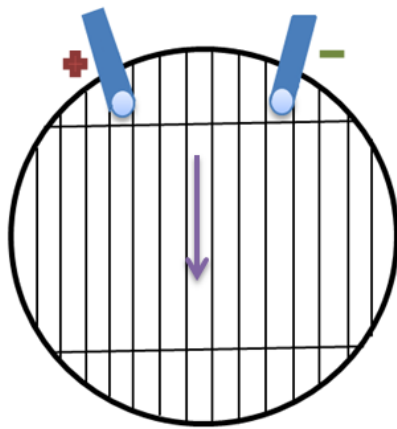


Fig. 17. Optical mapping of tissue culture.

A



B

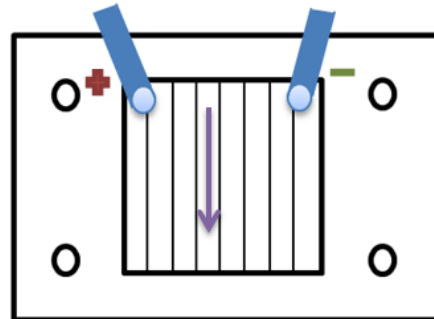


Fig. 18. p35 (A) and silicon well (B) for optical mapping with stimulation electrodes (blue) and impulse propagation direction (purple).

Control of the optical mapping system and data storage was performed with custom software in Matlab previously developed in the laboratory, and analysis of the fluorescent images was carried out in a specialized developed Guided User Interface. By introducing the file containing the image sequence recorded with the optical mapping system, and selecting two pixels, the program gives a value for conduction velocity between these two pixels. The program correlates the two fluorescent signals obtained, and with a calibration distance (spatial

information) previously indicated and the electric impulse correlation distance (temporal information), conduction velocity is calculated. This process can be observed in **Fig. 19**.

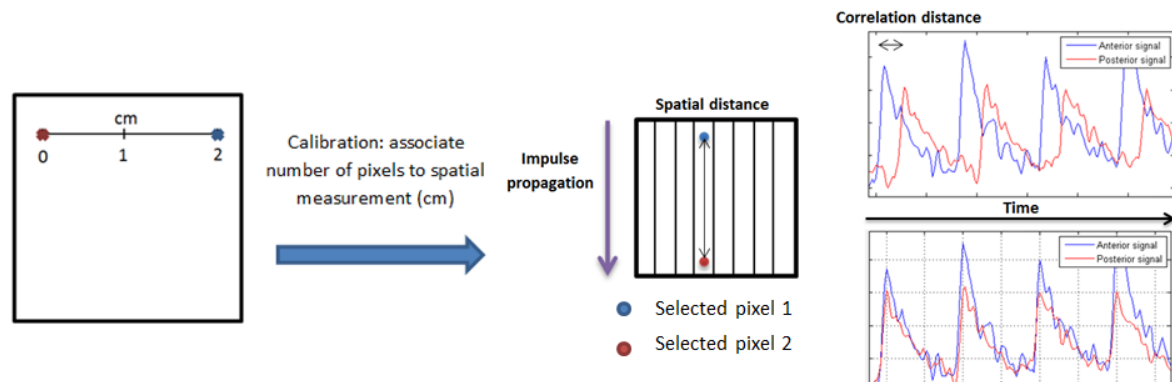


Fig. 19. Process for calculating conduction velocity. (1) Calibration. (2) Pixel selection. (3) Correlation of fluorescent signal in time of pixel 1 and pixel 2 (4) Calculate conduction velocity as Spatial distance (cm)/Correlation distance (s).

Analysis of gene expression

To study changes at a molecular level, a quantitative PCR was performed on three Petri dish and three silicon well samples. The first step was to extract RNA from HL-1 cells grown in the two substrates after full confluence (three p35s and three silicon wells). To carry out RNA extraction following phenol-chloroform procedure, cells were resuspended in 1 ml of Tri-reagent (Sigma) and the mixture was homogenised. 200 µl of chloroform were added and it was vortexed for 15 seconds. After leaving it 15 minutes at room temperature, the solution was centrifuged at 12000xg during 15 minutes. Later on, the upper aqueous phase containing RNA was carefully collected (DNA and proteins precipitate stayed at the interphase), and 500 µl of isopropanol were added. After inverting several times, RNA was left to precipitate 15 min at room temperature. It was centrifuged again at 12000xg during 15 min and supernatant was eliminated. It was later washed with ethanol, left dry and resuspended in 20 µl of H₂O RNase-free. RNA was quantified in the Nanodrop (Nanophotometre Pearl, IMPLEN, bioNova cientifica) to check RNA quality and quantity that needed to be placed to obtain uniform RNA concentration for all the samples.

Transcripts were quantified in a two-step RT-PCR. First strand cDNA was synthesized using High Capacity cDNA Reverse Transcription Kit (Applied Biosystems). Then, in order to prepare the qPCR reaction, a total volume of 25 µl per well was prepared as follows: 12 µl of Power SYBR Green® (mix of fluorophore and polymerase-enzyme from Applied Biosystems), 0.5 µl of cDNA of my sample, 11.5 µl of H₂O RNase-free, 0.5 µl of forward primer and 0.5 µl of reverse primer. Specific primers used for the amplification of a small region (around 150-350 base pairs) of the gene of interest can be observed in **Table 2**.

Gene	Protein	Forward Primer (5'→3')	Reverse Primer (5'→3')
SCN5A	Nav 1.5	CACCTTCACCGCCATCTACA	AAGGTGCGTAAGGCTGAGAC
CACNA1C	Cav 1.2	CCTCGAAGCTGGGAGAACAG	TGTGTGGGAGTCAATGGAGC
KCNJ2	Kir 2.1	GACGCCTTCATCATTGGTGC	CCGGACATGAGCTTCCACAA
GJA5	Con 40	ATACCATTGAGCCTGGTTGC	GGTGGGCCTCTTTAGCTTTC
GJA1	Con 43	GGACTGCTTCCTCTCACGTC	CAGCTTGTACCCAGGAGGAG
GJA7	Con 45	TTTGTGTGCAACACAGAGCA	GGTCCTCTCCGTTTCTTCC
36B4		GCGACCTGGAAGTCCAATA	ATCTGCTGCATCTGCTTGG
CYCLOPHYLIN		ACAGGTCTGGCATCTTGTC	CATGGCTTCCACAATGTTCA

Table 2. Primers used for reverse transcription polymerase chain reaction (RT-PCR).

The samples were run using CFX Real Time PCR detection Systems (Bio-Rad). Two biological replicates per target gene were used, and two technical replicates for each sample. Gene expression values were obtained using the $2^{-(\Delta\Delta C(T))}$ method (**Appendix 3: $2^{-(\Delta\Delta C(T))}$**), normalizing with two standard housekeeping genes (36b4 and Cyclophilin).

The programmed cycles are: Initial cycle of 95°C during 10 min, 40 cycles at 95°C during 15 s and 60°C during 1 min, and final melting curve to know if primers are still working of 95°C during 15 s, 60°C during 15 s, ramp of 20 min and 95°C during 15 s.

Expenditure

The estimation of the total cost of the project results from the sum of costs of personnel, the cost of the materials needed for the cell culture and the costs of each of the tests. The costs for the cell culture in each of the substrates can be observed in **Table 3**. The costs for each of the tests performed can be observed in **Tables 4-7**. The cost of the use of the equipment required is calculated according to its depreciation value obtained from the total unit costs, the life span of the product and the time it was used.

Cell culture expenditure											
Material	Unit Price	Volume of Claycomb medium needed per unit	Claycomb medium price per unit (0.23 €/ml)	Other lab material expenses (pipettes, syringes, filters...)	Total maintenance cost per well	Units required for the experiment					Total costs
						Proliferation test	Migration and displacement test	Electrophysiological properties test	Analysis of gene expression	Total units required	
PDMS silicon well	10 €	9 ml	2.10 €	2 €	14.10 €	3	3	4	3	13	183 €
P35 Petri dish	0.19 €	12 ml	2.80 €	2€	5 €	3	3	4	3	13	65 €
Total											248 €

Table 3. Expenses of cell culture.

Proliferation tests expenditure						
Equipment depreciation per test	Average alamarBlue® quantity per test and day	Expenses of alamarBlue® per test and day (7€/ml)	Number of tests	Number of days	Total alamarBlue® expenses	Total cost
1.5 €	125 µl	0.88 €	6	3	15.80 €	24.8 €

Table 4. Proliferation tests expenditure.

Migration and displacement tests expenditure			
Equipment depreciation/test (1 week duration)	Number of tests	Matlab license (6 months)	Total cost
14 €	6	125 €	209 €

Table 5. Migration and displacement tests expenditure.

Optical mapping tests expenditure				
Equipment depreciation per test	Fluorescent probes, chemical reagents and other materials	Total cost per test	Number of tests	Total cost
10 €	3€	13 €	8	104 €

Table 6. Optical mapping tests expenditure.

Analysis of gene expression (qPCR) expenditure							
Equipment depreciation test per sample	RNA extraction reagents per sample	Reverse Transcriptase Kit per sample	Primers per sample	SYBR® Green per sample	Total cost per sample	Number of samples	Total cost
4 €	15 €	5 €	0.8€	3.2 €	28 €	6	168€

Table 7. Analysis of gene expression tests expenditure.

The total costs for the materials and methods employed in cell culture and in performing the different tests can be seen in **Table 8**.

Total material and equipment costs						
Cell culture	Proliferation test	Migration and displacement test	Optical mapping test	Analysis of gene expression (qPCR)	Other costs (PC depreciation, Microsoft Office...)	Total cost
248 €	25 €	209 €	104 €	168 €	200 €	954 €

Table 8. Total material and equipment costs.

The total personnel costs of the project can be seen in **Table 9**.

Total personnel costs			
Personnel	Personnel cost (€/hour)	Hours	Total cost
Biomedical Engineer	20	400	8000 €
Project collaborator	35	80	2800 €
Project coordinator	35	80	2800 €
Total			13600 €

Table 9. Total personnel costs.

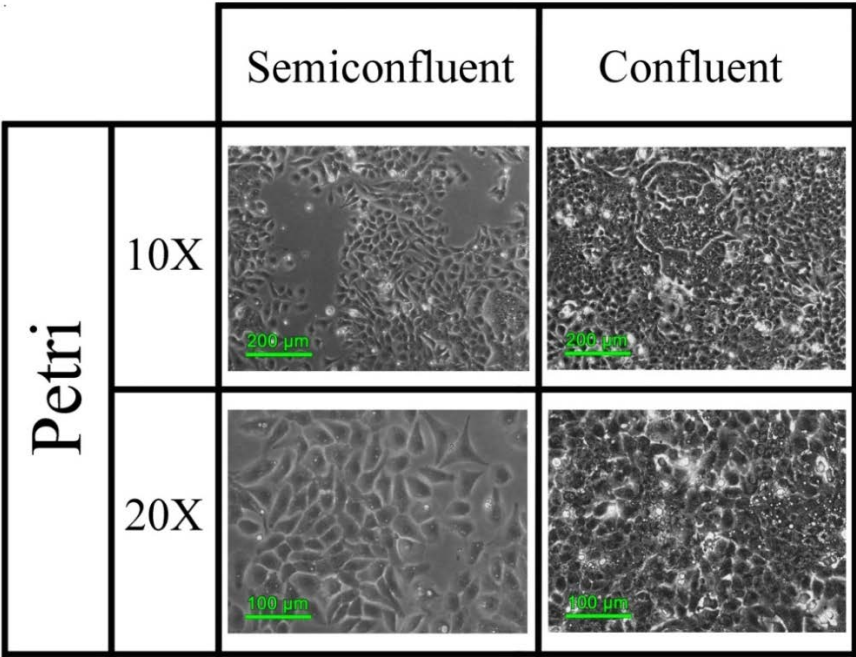
Summing both the costs of personnel and the costs of the materials and equipment employed, the total costs of the project is **14554 €**.

In this section, the results for the different properties studied in both substrates are shown. The cells were able to grow and keep spontaneous contraction during cell culture. Proliferation showed to be better at early stages of cell culture in Petri and in silicon during late stages, and migration and displacement in HL-1 cells were very low in both substrates. Regarding electrophysiological properties, conduction velocity showed better results in silicon wells than in Petri dishes, and analysis of gene expression also confirmed what observed at functional level, as genes codifying for proteins involved in impulse generation and conduction were more expressed in silicon wells.

Cell culture

The result for the cell culture test was satisfactory, as cells attached and grew on both substrates. In **Fig. 20**, images of the different substrates at different confluence levels and with different objectives are shown. In the images it can be observed how cells grow similarly in both substrates and how they suffer the same change in morphology from the semiconfluence to the full confluence state.

A



B

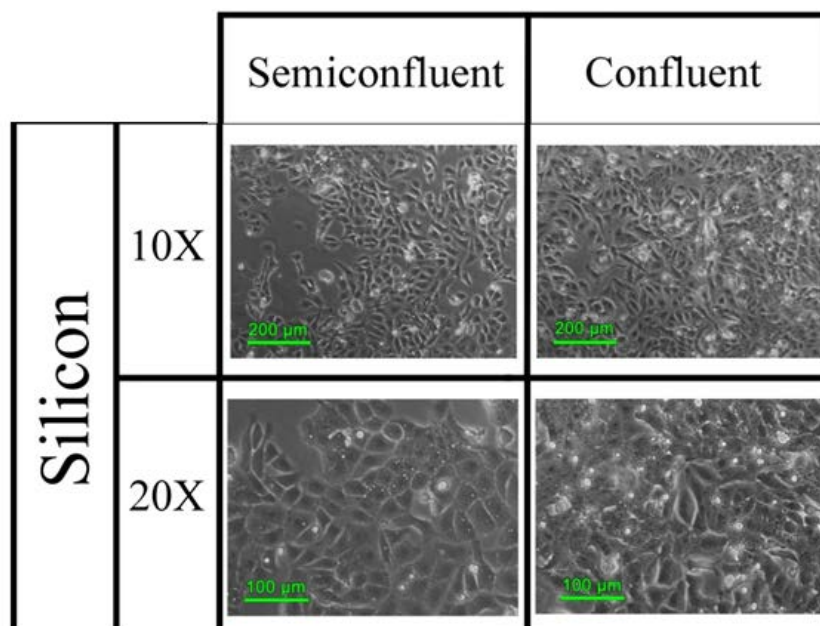


Fig. 20. HL-1 images at different confluence levels in Petri dishes (A) and in silicon wells (B).

Proliferation

After incubating alamarBlue®, a change in the colour of the media was observed (**Fig. 21**). Pinker colours correspond to a higher reduction of the medium, and so, to a higher proliferation. Bluer colours correspond to more intact medium, so less proliferation.



Fig. 21. Colorimetric changes produced by alamarBlue® reduction in Petri (P) and silicon wells (S). White is represented by letter B (medium without cells). (+), (~) and (-) correspond to the different initial concentrations indicated in **Table 1**.

In the following figure (**Fig. 22**) it is shown the percentage of reduction calculated from measured absorbance by applying the formula explained in the methods section.

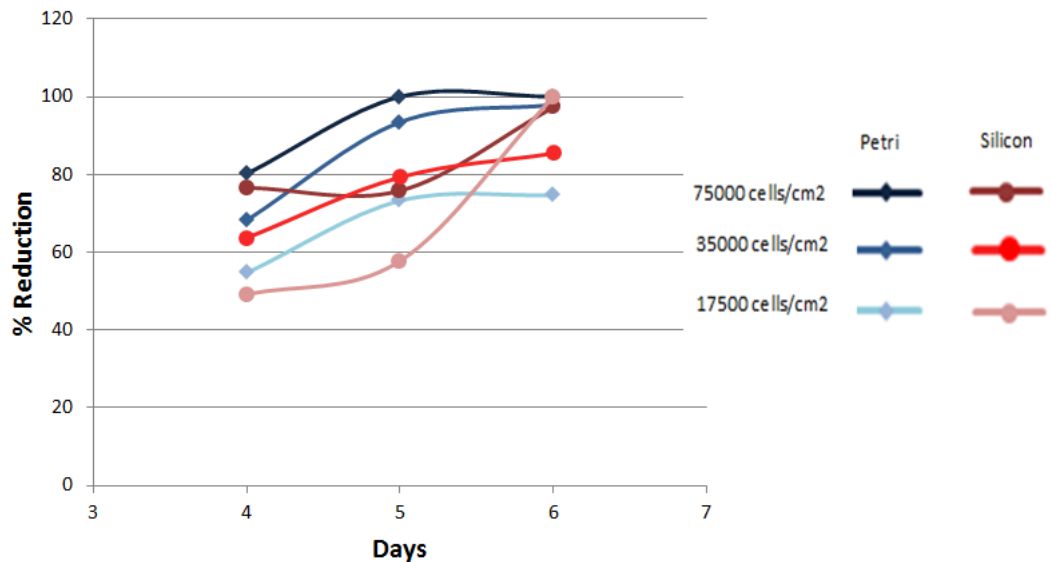


Fig. 22. Proliferation in time in both substrates (Petri and Silicon) at different initial concentrations.

As it can be observed in the previous figure, proliferation took shorter to reach a maximum value when HL-1 were grown over Petri and the starting concentration was high (0.75×10^6 and 0.35×10^6) as they reach full confluence in five days. It is also important to note that at lower concentrations, silicon wells proliferate at a very low rate, but that it increased as cell concentration got higher. In the curves corresponding to initial concentrations of 0.175×10^6 and 0.35×10^6 in silicon, proliferation rate is much higher from day five to six than from day four to five. This suggests that in silicones, performance gets better in time.

In Petri dishes a more reproducible response can be observed as the three curves corresponding to the three different starting cell concentrations show exactly the same shape. However, in silicon wells a very diverse response is shown depending on the initial concentration. This supports our observation that in silicon wells response is neither as stable nor predictable. In order to get a clearer image, the previous results were normalized by the initial concentration and merged in one unique curve, with bar errors corresponding to the standard deviation between the three curves (**Fig. 23**).

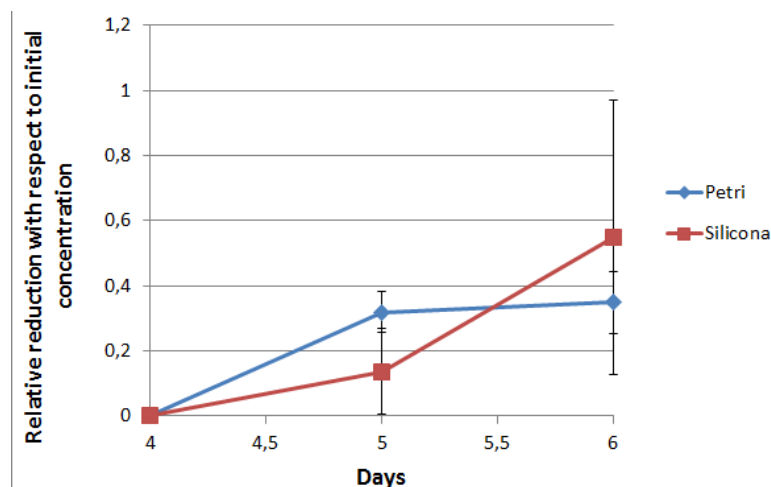


Fig. 23. Relative reduction with respect to initial concentration over time.

Standard deviation is greater in silicon measurements, as there is more variability. In Petri, higher proliferation rate is shown at early stages while in silicon highest proliferation rate occurs at late stages.

Migration and displacement

The ability of HL-1 to close induced wounds showed to be very low. After 60 hours, none of the injuries were completely closed in any of the materials, nor using the stencil neither scratching with the pipette. In **Fig. 24** one representative wound in each of the substrates is shown at the beginning of the test and 30 and 60 hours later. It can be observed how wounds did not close completely.

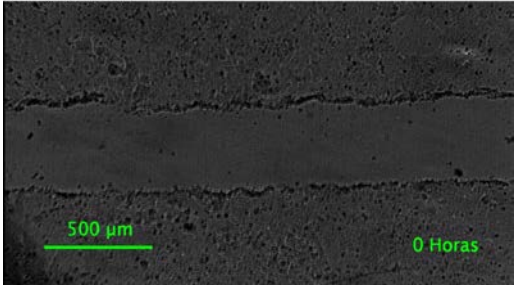
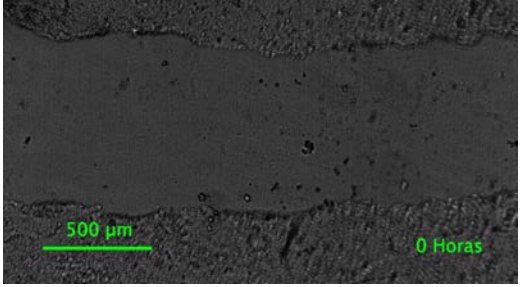
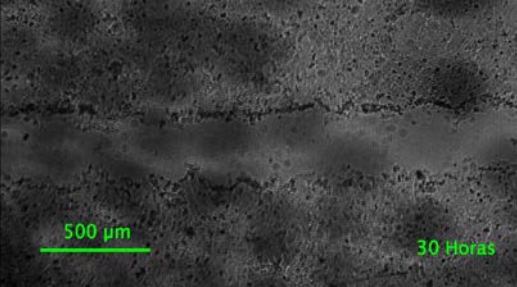
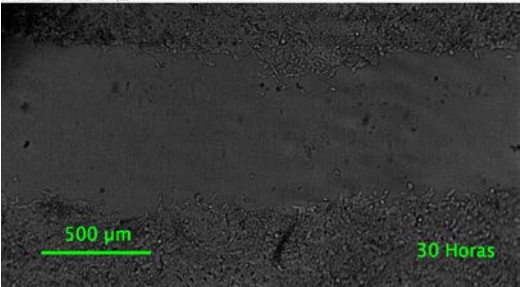
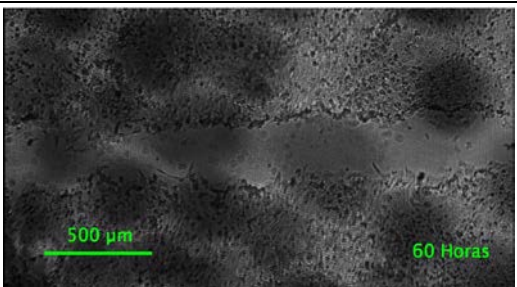
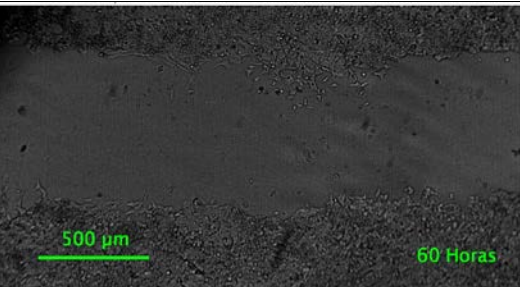
Time	Petri	Silicon
0 hours		
30 hours		
60 hours		

Fig. 24. Wound test results in Petri and Silicon.

To obtain confluence information over time from image sequences, the custom software developed (Time-lapse analyser) was used. For further software details, check **Appendix 1: Migration and displacement software package**. The videos obtained were also generated by using the software package developed during the present study. The interface can be observed in **Fig. 25**.

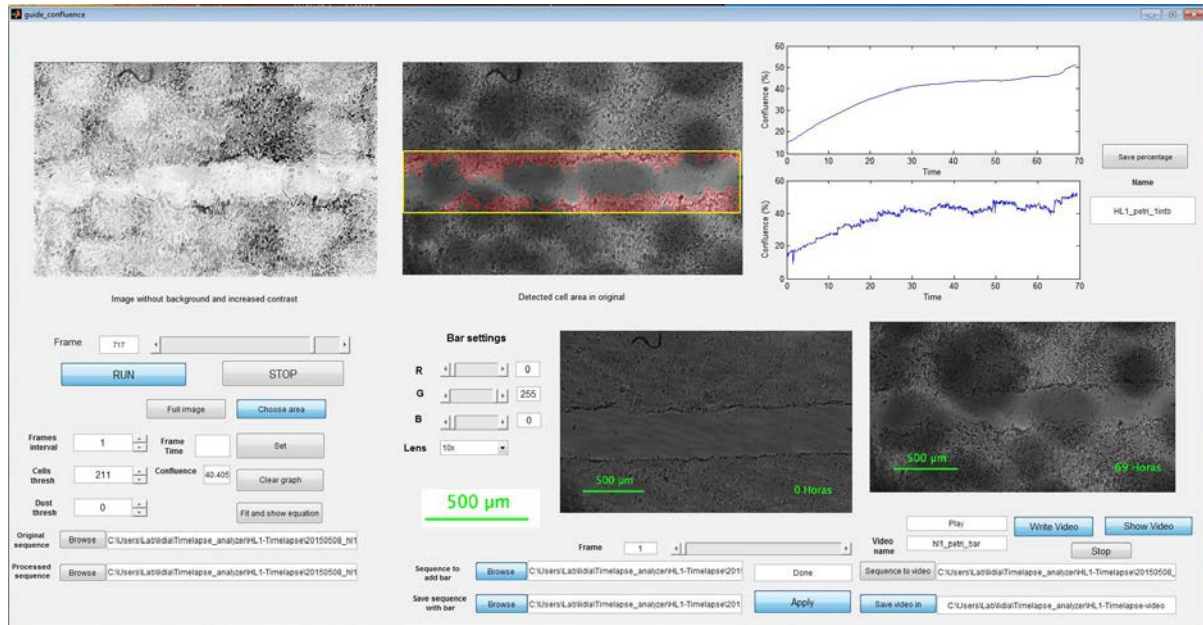


Fig. 25. Time-lapse analyser interface.

The confluence graph obtained in the wound area with the Time-lapse Analyser is shown in **Fig. 26**.

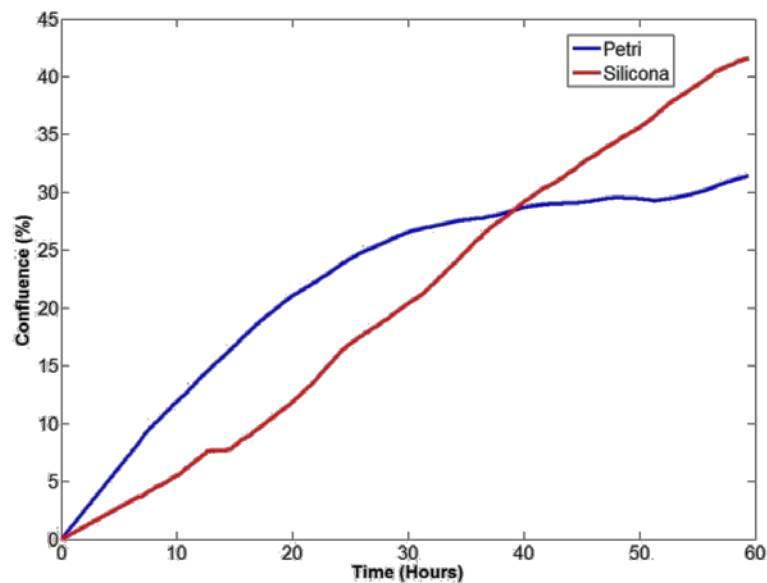


Fig. 26. Wound area covered with cells in time in both substrates.

From the wound test images and from the aforementioned graph, it can be inferred that HL-1 do not show large migration capacity. It is interesting to note that this graph keeps a direct relationship with the one in **Fig. 23**. Again, cardiac cells seem to grow faster in Petri in the early stages and faster in silicon at the late stages. The similarity between both graphs and the way in which cells cover the cell area (moving in groups more than spreading over the wound area) suggest that these cells colonize only by proliferation. That is, that cells near the interface divide and new cells attach in the free space next to them, but do not move further apart. In fact, the analysis of maximum displacement velocities (i.e. $0.06 \mu\text{m/s}$ in silicon and $0.04 \mu\text{m/s}$ in Petri) demonstrated the reduced ability to migrate of these adult cardiomyocytes.

Electrophysiological properties

Electric impulses were able to generate and transmit in both substrates. Thus, conduction velocity was calculated for different bands in each of the samples with the developed software. It also included the option of performing isochrone maps. For further software details go to **Appendix 2: Electrophysiology analyser software**. The interface can be observed in **Fig. 27**.

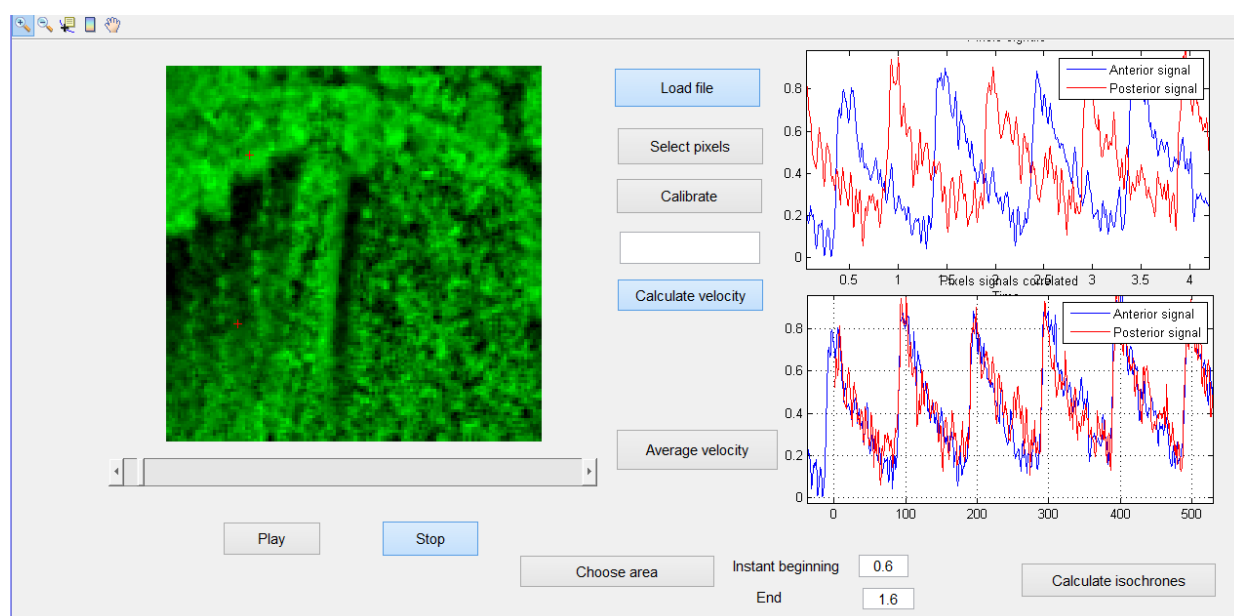


Fig. 27. Electrophysiology analyser Interface.

The average conduction velocity of the four samples grown in Petri dishes and of the four samples grown in silicon wells can be observed in **Fig. 28**. The conduction velocity is 156% greater in silicon wells (2.4 cm/s) than in Petri dishes (1.5 cm/s). Although these results are still far from mimicking real *in vivo* conduction velocities, there is a substantial increase in the impulse propagation velocity. This can be explained by the fact that flexibility of silicon wells have closer mechanical properties to ECM, so cells develop a more differentiated cardiac phenotype.

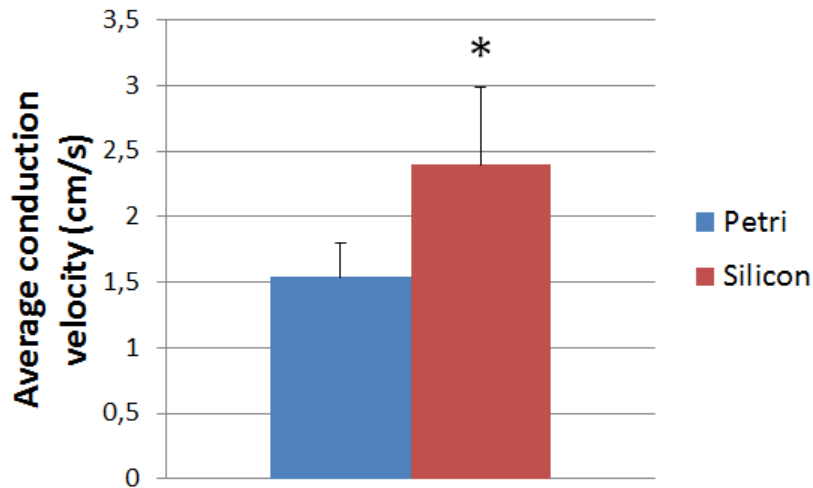


Fig. 28. Average conduction velocity for each substrate. Differences are statistically significant when $p < 0.05$ (*) (TTest).

In the following figure (**Fig. 29**), an isochrones map for one selected significant band in Petri and silicon can be observed. Impulse takes shorter to reach the end of the band in silicon than in the Petri dish, suggesting faster conduction velocities. Uniform impulse propagation can be observed in both bands, confirming that cells were confluent and that conduction followed a straight path.

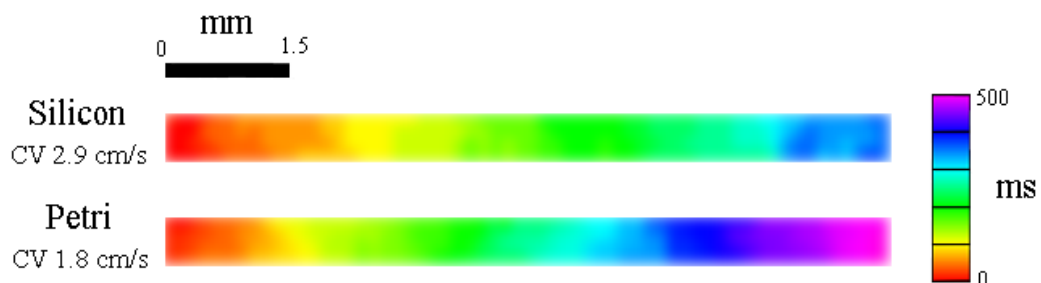


Fig. 29. Isochrone maps of a significant band in each substrate.

Analysis of gene expression

After performing the qPCR with three HL-1 samples grown in silicon and three samples grown in Petri and analysing the results, the relative gene expression of different genes codifying for proteins involved in action potential generation and propagation can be observed. Petri dish samples are taken as the reference in **Fig. 30** and **Fig. 31**.

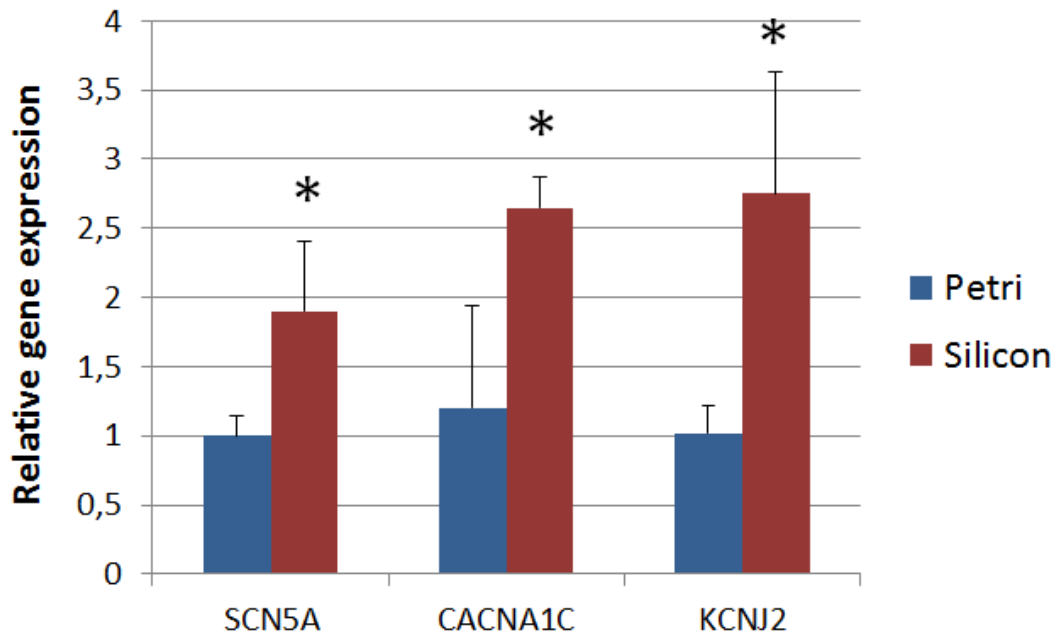


Fig. 30. Expression levels of ion channels in HL1 cells grown in silicon versus Petri substrates. SCN5A, CACNA1C and KCNJ2 genes codify for proteins which are subunits of ion channels associated to I_{Na} , I_{CaL} and I_{K1} respectively. Differences are statistically significant when $p < 0.05$ (*) (TTest).

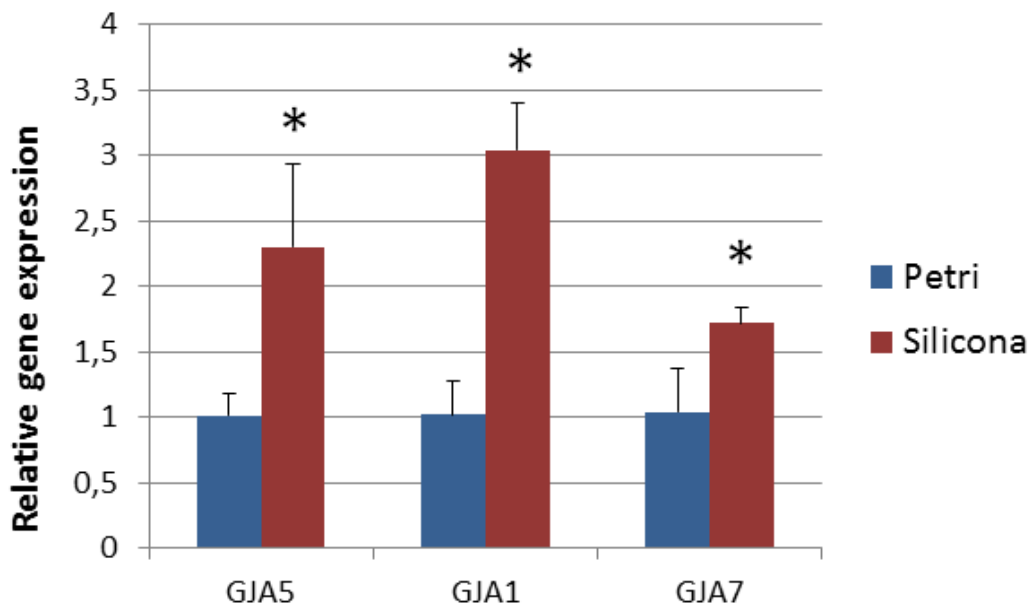


Fig. 31. Expression levels of connexin genes in HL1 cells grown in silicon versus Petri substrates. GJA5, GJA1, GJA7 genes codify for components of the gap junctions: connexin 40, connexin 43 and connexin 45 respectively. Differences are statistically significant when $p < 0.05$ (*) (TTest).

These results support what is observed at a functional level when comparing conduction velocity values. A higher expression of genes codifying for molecular components of sodium, calcium and potassium channels (**Fig. 30**) and of genes codifying for connexins forming part of gap junctions (**Fig. 31**), may indicate a greater presence of these proteins in HL-1 cells, which will explain this higher conduction velocities. These results confirm the influence of the flexible substrate on electrophysiological cardiomyocytic properties driven by changes in gene expression, which are probably associated to the mechanical similarity of the silicon wells with the *in vivo* environment of cardiac cells.

Main contributions

The results of this study confirm that the culture of cardiac cells on flexible membranes has an impact on their phenotype. This impact has shown to be especially significant in electrophysiological properties, as conduction velocity has increased considerably. One possible justification for this is that the similarity of the Young Modulus of PDMS with that of the ECM has triggered a gene expression profile more characteristic of adult cardiomyocytes, and these changes in gene expression can lead to a higher presence of gap junctions and ion channels that ease impulse generation and propagation. Proliferation, migration and displacement have not shown such significant differences between both substrates, but in silicon wells these properties intensify more than in Petri dishes.

The use of flexible membranes opens new insights into cardiac patches for cardiac regeneration, as obtaining higher conduction velocities while maintaining other general cell properties is possible. As impulses propagate faster, the possibility of future re-entries will diminish and the patch will integrate better within healthy tissue. Flexible membranes also allow future studies of electrophysiological properties of cell cultures under mechanical and electrical stimulation at the same time, which is otherwise impossible with rigid Petri dishes. These conditions may improve characteristic cardiomyocytes properties even further, leading to better quality patches.

This study has also resulted in the development of custom software for future analysis of these properties in other studies performed at the Laboratory. The first one allows processing time-lapse images acquired. It allows obtaining confluence information in time by segmenting cells from the background in a user selected area in order to follow wound closure, and also to obtain displacement velocity by tracking a cell. It also includes the possibility of making videos from image sequences with spatial scale and time code for future studies. The second one is intended to obtain conduction velocity values over optical mapping images in a reliable and accurate manner, which is a common procedure when analysing electrophysiological properties. It also performs isochrones maps that ease comprehension of the results obtained and summarize in an image how impulse propagates over the studied area.

Comparison with previous studies

The use of flexible membranes has already been suggested to have an impact on impulse propagation. Conduction velocities in rat ventricular myocyte monolayers are between 20 and 25 cm/s. However, *in vitro* growing of cardiac cell lines and iPSCs has shown very inferior speeds (1-2.5 cm/s). The maximum conduction velocity obtained *in vitro* has been increased up

to 21 cm/s using genetically purified human cardiac myocytes and using flexible membranes [30], however, the impact of flexible membranes alone on electrophysiological properties has not been quantified before.

Cardiac patches made up from decellularized matrix also seem promising in keeping adult cardiomyocytic properties [85]. They have retained biochemical, structural and mechanical aspects of extracellular matrix and cardiomyocytes are able to align and show anisotropic properties inherent in native tissue. Using these decellularized matrices and neonatal rat ventricular cells, conduction velocities of 14.5 cm/s have been reached [86].

The high conduction velocities obtained in these studies may be partly due to the use of flexible membranes and partly due to the types of cells used. With this work it was demonstrated and quantified that flexible membranes are responsible for increases in the conduction velocity. General cell properties studied here such as proliferation, migration and displacement had not been quantified in HL-1 cells in flexible and rigid materials before, and this gives valuable information on some of the strengths and limitations of this cell line for their use as models and for cardiac patches generation.

Clinical applications

The generation of cardiac patches that mimic *in vivo* properties have two main applications: (1) as therapy for cardiac regeneration of scar tissue after a heart attack and (2) as models of cardiac tissue for drug and therapy testing. Although the first application still needs to overcome some limitations to reach the clinical practice, current research offers optimistic insights into cardiac patches as therapy. The use of these patches as realistic models of in-vivo behaviour offer many advantages. First, they reduce the number of animals required for the experiment and thus save many costs. Secondly, they reduce the time required to perform the experiments, they provide more reliable results and they ease the procedure.

The developed software also contributes to cardiac patch evaluation by quantifying the different properties assessed in this work. They present high versatility as they work for any cell type, drug and testing conditions as long as the tests are carried out with the same or similar equipment. Thus, Guided User Interfaces created allow confluence, displacement and conduction velocity studies for comparison of different drugs and cell culture conditions in an intuitive way, with the aim of determining the factors that lead to desired results.

Limitations

One of the main limitations of the procedure carried out is the use of gene expression as a marker for protein presence. Although this helps to have a general idea of what happens at the molecular level and helps support functional behaviour observed, in order to confirm protein presence specific and direct techniques to detect them should be used for confirmation.

The results obtained for conduction velocity, although higher for flexible membranes, are still far from *in vivo* impulse propagation velocities, which may present limitations for their use as accurate models and patches. In order to reach higher conduction velocities, differentiated iPSCs or primary cells should try to be used (if possible of human origin). The use of decellularized matrices could also contribute to improve cardiomyocytic properties, as it provides an ideal environment for cells to grow. Another key limitation for this kind of cells to be used for cardiac patch generation is the low migration and displacement velocity obtained. The low ability of adult cardiac myocytes to close wounds may limit their use for this purpose considerably. In order to solve it, immature cardiomyocytes such as cardiopoietic cells or iPSCs not terminally differentiated into cardiomyocytes should be contemplated.

Future work

The next steps that should be followed in order to create tissue engineered optimum patches is to assess the properties studied here in decellularized matrix. If the results continue being satisfactory, new cell types should be tried, such as differentiated iPSCs of human origin. Some protein direct detection technique should also be added to the tests performed here.

In the next months, an article will be presented in the XXXIII Congress of the Spanish Society of Biomedical Engineering (CASEIB 2015) with the results obtained in this study. In addition to that, the work will be further improved to be sent to the 37th Annual International Conference of the IEEE Engineering in Medicine and Biology Society, and the process to prepare the manuscript for publication in Journal Citation Reports (JCR) will be initiated.

Regarding the software, the platform could be made more automated and less user-interactive. The electrophysiology analyser interface could be improved by identifying bands and calculating conduction velocity in several areas and of several films at once without requiring user intervention. It could also add the possibility of measuring action potential duration. The time-lapse analyser interface could be improved by automatically improving contrast in the image and by incorporating the option of automatic thresholding that provides desired results.

Conclusions

The comparison between rigid Petri dishes and flexible membranes during the culture of HL-1 cells for the different general cell properties and specific cardiomyocytic properties was carried out successfully, and significant differences were observed.

- General cell properties involved in cardiac regeneration were proliferation, migration and displacement
 - Proliferation was in general very high because of the nature of the cells used. It was slightly higher at early stages of the culture in Petri, while at later stages it was higher in silicon wells. Flexible membranes also exhibited more variability and thus less reproducibility.
 - Migration and displacement of the cardiac cells were low in both substrates as it is characteristic of adult cardiomyocytes. From the data observed, it could be concluded that HL-1 cells colonize merely by proliferation. This low ability to repair wounds may pose further problems for the generation of cardiac patches, so it should be further studied.
 - The developed software for the analysis of time-lapse images was user-friendly and fast. It allowed successfully the obtaining of confluence graphs, displacement velocity and videos with time code and spatial scale.
- Specific cell properties analysed were conduction velocity and expression of genes related to action potential generation and propagation
 - In both substrates, HL-1 cells retained their phenotype and kept spontaneous contractile properties and impulse generation and propagation.
 - At the functional level, conduction velocity values were significantly higher when cells were cultured in silicon wells. At the molecular level, expression of genes coding for proteins involved in ion channels and gap junctions were also more expressed in flexible membranes, supporting the previous results.
 - The custom software generated is intuitive and serves its purpose effectively.

The use of flexible membranes has shown to play a role in cardiac cell phenotype, especially inducing better impulse propagation. This opens new insights into cardiac patches, as its use allows further research on the impact of continuous electrical and mechanical stimulation during cell culture and they mimic better *in vivo* characteristics of cardiac cells.

Bibliography

1. Gaziano T, Reddy KS, Paccaud F, Horton S, Chaturvedi V. Cardiovascular Disease. In: Jamison DT, Breman JG, Measham AR, Alleyne G, Claeson M, Evans DB, et al., editors. *Disease Control Priorities in Developing Countries*. 2nd ed. Washington (DC): World Bank; 2006.
2. Affluence and the Worldwide Distribution of Cardiovascular Disease Risks. *PLoS Med*. 2005 May.
3. Statistics - Heart and Stroke Foundation of Canada. heartandstroke.ca.
4. Chilnick LD. *The First Year: Heart Disease: An Essential Guide for the Newly Diagnosed*. Da Capo Press; 2009. 569 p.
5. McMurray JJV, Pfeffer MA. Heart failure. *Lancet Lond Engl*. 2005 Jun 28;365(9474):1877–89.
6. Smolina K, Wright FL, Rayner M, Goldacre MJ. Long-Term Survival and Recurrence After Acute Myocardial Infarction in England, 2004 to 2010. *Circ Cardiovasc Qual Outcomes*. 2012 Jul 1;5(4):532–40.
7. Wang B, Borazjani A, Tahai M, Curry AL de J, Simionescu DT, Guan J, et al. Fabrication of cardiac patch with decellularized porcine myocardial scaffold and bone marrow mononuclear cells. *J Biomed Mater Res A*. 2010 Sep 15;94(4):1100–10.
8. Rubio Guivernau JL, Ledesma Carbayo MJ, Arenal Maíz Á, Hernández J, Pérez David E, Fernández Avilés F. Do the spatial characteristics of myocardial scar tissue determine the risk of ventricular arrhythmias? *Cardiovasc Res*. 2012 Mar 1;94(10.1093/cvr/cvs113):324–32.
9. Palchesko RN, Zhang L, Sun Y, Feinberg AW. Development of Polydimethylsiloxane Substrates with Tunable Elastic Modulus to Study Cell Mechanobiology in Muscle and Nerve. *PLoS ONE*. 2012 Dec 11.
10. Li R-K, Weisel RD. *Cardiac Regeneration and Repair: Biomaterials and Tissue Engineering*. Elsevier; 2014. 509 p.
11. Severs NJ. The cardiac muscle cell. *BioEssays News Rev Mol Cell Dev Biol*. 2000 Feb;22(2):188–99.
12. Claycomb WC, Lanson NA, Stallworth BS, Egeland DB, Delcarpio JB, Bahinski A, et al. HL-1 cells: a cardiac muscle cell line that contracts and retains phenotypic characteristics of the adult cardiomyocyte. *Proc Natl Acad Sci U S A*. 1998 Mar 17;95(6):2979–84.
13. OCAL. Graphic of a Myocardiocyte (Heart Muscle Cell), including organelles and cell membrane functions. 2013.
14. Jalife J, Delmar M, Anumonwo J, Berenfeld O, Kalifa J. *Ion Channels. Basic Cardiac Electrophysiology for the Clinician*. Wiley-Blackwell; 2009. p. 43–71.

15. McNair WP, Ku L, Taylor MRG, Fain PR, Dao D, Wolfel E, et al. SCN5A mutation associated with dilated cardiomyopathy, conduction disorder, and arrhythmia. *Circulation*. 2004 Oct 12;110(15):2163–7.
16. Catterall WA, Perez-Reyes E, Snutch TP, Striessnig J. International Union of Pharmacology. XLVIII. Nomenclature and structure-function relationships of voltage-gated calcium channels. *Pharmacol Rev*. 2005 Dec;57(4):411–25.
17. Jalife J, Delmar M, Anumonwo J, Berenfeld O, Kalifa J. Impulse Initiation and Propagation in Cardiac Muscle. *Basic Cardiac Electrophysiology for the Clinician*. Wiley-Blackwell; 2009.
18. Kubo Y, Adelman JP, Clapham DE, Jan LY, Karschin A, Kurachi Y, et al. International Union of Pharmacology. LIV. Nomenclature and molecular relationships of inwardly rectifying potassium channels. *Pharmacol Rev*. 2005 Dec;57(4):509–26.
19. College O. Illustration from Anatomy & Physiology, Connexions Web site. Jun 19, 2013.
20. Blausen com staff “Blausen gallery 2014”. The sodium-potassium pump and related diffusion of sodium and potassium between the extracellular and intracellular space. 2014.
21. Fishman GI, Eddy RL, Shows TB, Rosenthal L, Leinwand LA. The human connexin gene family of gap junction proteins: distinct chromosomal locations but similar structures. *Genomics*. 1991 May;10(1):250–6.
22. Homo sapiens gap junction protein, alpha 5, 40kDa (GJA5), transcript variant B, mRNA. 2015 Mar 15.
23. Kanter HL, Saffitz JE, Beyer EC. Molecular cloning of two human cardiac gap junction proteins, connexin40 and connexin45. *J Mol Cell Cardiol*. 1994 Jul;26(7):861–8.
24. CNX O. Anatomical illustration of Cardiac muscle. 2013.
25. Stett A, Bucher V, Burkhardt C, Weber U, Nisch W. Patch-clamping of primary cardiac cells with micro-openings in polyimide films. *Med Biol Eng Comput*. 2003 Mar;41(2):233–40.
26. Cell culture systems and in vitro toxicity testing. Technical report no. 4 of the Johns Hopkins Center for Alternatives to Animal Testing (CAAT): technical workshop of June 13–15, 1990. *Cytotechnology*. 1992;8(2):129–76.
27. White SM, Constantin PE, Claycomb WC. Cardiac physiology at the cellular level: use of cultured HL-1 cardiomyocytes for studies of cardiac muscle cell structure and function. *Am J Physiol Heart Circ Physiol*. 2004 Mar;286(3):H823–9.
28. Bethesda, MD: National Institutes of Health, U.S. Department of Health and Human Services, 2015. Stem Cell Information.
29. Takahashi K, Yamanaka S. Induction of pluripotent stem cells from mouse embryonic and adult fibroblast cultures by defined factors. *Cell*. 2006 Aug 25;126(4):663–76.

30. Lee P, Klos M, Bollensdorff C, Hou L, Ewart P, Kamp TJ, et al. Simultaneous voltage and calcium mapping of genetically purified human induced pluripotent stem cell-derived cardiac myocyte monolayers. *Circ Res*. 2012 Jun 8;110(12):1556–63.
31. Nunes SS, Miklas JW, Liu J, Aschar-Sobbi R, Xiao Y, Zhang B, et al. Biowire: a platform for maturation of human pluripotent stem cell-derived cardiomyocytes. *Nat Methods*. 2013 Agosto;10(8):781–7.
32. Saha K, Jaenisch R. Technical challenges in using human induced pluripotent stem cells to model disease. *Cell Stem Cell*. 2009 Dec 4;5(6):584–95.
33. Mummery CL, Zhang J, Ng ES, Elliott DA, Elefanty AG, Kamp TJ. Differentiation of Human Embryonic Stem Cells and Induced Pluripotent Stem Cells to Cardiomyocytes A Methods Overview. *Circ Res*. 2012 Jul 20;111(3):344–58.
34. Irfan Maqsood M, Matin MM, Bahrami AR, Ghasroldasht MM. Immortality of cell lines: challenges and advantages of establishment. *Cell Biol Int*. 2013 Oct 1;37(10):1038–45.
35. Senyo SE, Lee RT, Kühn B. Cardiac regeneration based on mechanisms of cardiomyocyte proliferation and differentiation. *Stem Cell Res*. 2014 Nov;13(3, Part B):532–41.
36. Yadav K, Singhal N, Rishi V, Yadav H. *Cell Proliferation Assays*. eLS. John Wiley & Sons, Ltd; 2001.
37. De Fries R, Mitsuhashi M. Quantification of mitogen induced human lymphocyte proliferation: Comparison of alamarblue™ assay to 3h-thymidine incorporation assay. *J Clin Lab Anal*. 1995;9(2):89–95.
38. Mead TJ, Lefebvre V. *Proliferation Assays (BrdU and EdU) on Skeletal Tissue Sections*. *Methods Mol Biol Clifton NJ*. 2014;1130:233–43.
39. Scholzen T, Gerdes J. The Ki-67 protein: from the known and the unknown. *J Cell Physiol*. 2000 Mar;182(3):311–22.
40. Riss TL, Moravec RA, Niles AL, Benink HA, Worzella TJ, Minor L. *Cell Viability Assays*. In: Sittampalam GS, Gal-Edd N, Arkin M, Auld D, Austin C, Bejcek B, et al., editors. *Assay Guidance Manual*. Bethesda (MD): Eli Lilly & Company and the National Center for Advancing Translational Sciences; 2004.
41. Quent VMC, Loessner D, Friis T, Reichert JC, Hutmacher DW. Discrepancies between metabolic activity and DNA content as tool to assess cell proliferation in cancer research. *J Cell Mol Med*. 2010 Apr;14(4):1003–13.
42. Hamid R, Rotshteyn Y, Rabadi L, Parikh R, Bullock P. Comparison of alamar blue and MTT assays for high through-put screening. *Toxicol Vitro Int J Publ Assoc BIBRA*. 2004 Oct;18(5):703–10.
43. Jain P, Worthylake RA, Alahari SK. Quantitative Analysis of Random Migration of Cells Using Time-lapse Video Microscopy. *J Vis Exp JoVE*. 2012 May 13.
44. Suuronen EJ, Ruel M. *Biomaterials for Cardiac Regeneration*. Springer; 2014. 333 p.

45. Itou J, Oishi I, Kawakami H, Glass TJ, Richter J, Johnson A, et al. Migration of cardiomyocytes is essential for heart regeneration in zebrafish. *Development*. 2012 Nov 15;139(22):4133–42.
46. Huth J, Buchholz M, Kraus JM, Mølhave K, Gradinaru C, v Wichert G, et al. TimeLapseAnalyzer: multi-target analysis for live-cell imaging and time-lapse microscopy. *Comput Methods Programs Biomed*. 2011 Nov;104(2):227–34.
47. Klein J, Leupold S, Biegler I, Biedendieck R, Münch R, Jahn D. TLM-Tracker: software for cell segmentation, tracking and lineage analysis in time-lapse microscopy movies. *Bioinforma Oxf Engl*. 2012 Sep 1;28(17):2276–7.
48. Jalife J, Delmar M, Anumonwo J, Berenfeld O, Kalifa J. *Bioelectricity. Basic Cardiac Electrophysiology for the Clinician*. Wiley-Blackwell; 2009. p. 7–42.
49. Efimov IR, Nikolski VP, Salama G. Optical imaging of the heart. *Circ Res*. 2004 Jul 9;95(1):21–33.
50. Lichtman JW, Conchello J-A. Fluorescence microscopy. *Nat Methods*. 2005 Dec;2(12):910–9.
51. Attin M, Clusin WT. Basic concepts of optical mapping techniques in cardiac electrophysiology. *Biol Res Nurs*. 2009 Oct;11(2):195–207.
52. Natarajan A, Stancescu M, Dhir V, Armstrong C, Sommerhage F, Hickman JJ, et al. Patterned Cardiomyocytes on Microelectrode Arrays as a Functional, High Information Content Drug Screening Platform. *Biomaterials*. 2011 Jun;32(18):4267–74.
53. Herron TJ, Lee P, Jalife J. Optical Imaging of Voltage and Calcium in Cardiac Cells & Tissues. *Circ Res*. 2012 Feb 17;110(4):609–23.
54. Nygren A, Baczkó I, Giles WR. Measurements of electrophysiological effects of components of acute ischemia in Langendorff-perfused rat hearts using voltage-sensitive dye mapping. *J Cardiovasc Electrophysiol*. 2006 May;17 Suppl 1:S113–23.
55. Kim YH, Xie F, Yashima M, Wu TJ, Valderrábano M, Lee MH, et al. Role of papillary muscle in the generation and maintenance of reentry during ventricular tachycardia and fibrillation in isolated swine right ventricle. *Circulation*. 1999 Sep 28;100(13):1450–9.
56. Comtois P, Kneller J, Nattel S. Of circles and spirals: bridging the gap between the leading circle and spiral wave concepts of cardiac reentry. *Eur Eur Pacing Arrhythm Card Electrophysiol J Work Groups Card Pacing Arrhythm Card Cell Electrophysiol Eur Soc Cardiol*. 2005 Sep;7 Suppl 2:10–20.
57. Bernard Valeur MNB-S. A Brief History of Fluorescence and Phosphorescence before the Emergence of Quantum Theory. *J Chem Educ - J CHEM EDUC*. 2011;88(6).
58. Jacobkhed. Jablonski diagram of absorbance, non-radiative decay, and fluorescence.. 2012.
59. Fluhler E, Burnham VG, Loew LM. Spectra, membrane binding, and potentiometric responses of new charge shift probes. *Biochemistry (Mosc)*. 1985 Oct 8;24(21):5749–55.

60. Wuskell JP, Boudreau D, Wei M, Jin L, Engl R, Chebolu R, et al. Synthesis, spectra, delivery and potentiometric responses of new styryl dyes with extended spectral ranges. *J Neurosci Methods*. 2006 Mar 15;151(2):200–15.
61. Rohr S, Salzberg BM. Multiple site optical recording of transmembrane voltage (MSORTV) in patterned growth heart cell cultures: assessing electrical behavior, with microsecond resolution, on a cellular and subcellular scale. *Biophys J*. 1994 Sep;67(3):1301–15.
62. Salama G, Choi B-R. Images of Action Potential Propagation in Heart. *News Physiol Sci Int J Physiol Prod Jointly Int Union Physiol Sci Am Physiol Soc*. 2000 Feb;15:33–41.
63. Takahashi A, Camacho P, Lechleiter JD, Herman B. Measurement of Intracellular Calcium. *Physiol Rev*. 1999 Jan 10;79(4):1089–125.
64. Hollingworth S, Gee KR, Baylor SM. Low-Affinity Ca^{2+} Indicators Compared in Measurements of Skeletal Muscle Ca^{2+} Transients. *Biophys J*. 2009 Oct 7;97(7):1864–72.
65. Fast VG. Simultaneous optical imaging of membrane potential and intracellular calcium. *J Electrocardiol*. 2005 Oct;38(4 Suppl):107–12.
66. Rudolf R, Mongillo M, Rizzuto R, Pozzan T. Looking forward to seeing calcium. *Nat Rev Mol Cell Biol*. 2003 Jul;4(7):579–86.
67. Paredes RM, Etzler JC, Watts LT, Lechleiter JD. Chemical Calcium Indicators. *Methods San Diego Calif*. 2008 Nov;46(3):143–51.
68. Del Nido PJ, Glynn P, Buenaventura P, Salama G, Koretsky AP. Fluorescence measurement of calcium transients in perfused rabbit heart using rhod 2. *Am J Physiol*. 1998 Feb;274(2 Pt 2):H728–41.
69. Choi B-R, Salama G. Simultaneous maps of optical action potentials and calcium transients in guinea-pig hearts: mechanisms underlying concordant alternans. *J Physiol*. 2000 Nov 15;529(Pt 1):171–88.
70. Andrew E. Moe SM. Improvements in LED-based fluorescence analysis systems. *Sens Actuators B Chem*. 2005;230–41.
71. Entcheva E, Bien H. Macroscopic optical mapping of excitation in cardiac cell networks with ultra-high spatiotemporal resolution. *Prog Biophys Mol Biol*. 2006 Oct;92(2):232–57.
72. Lee P, Bollensdorff C, Quinn TA, Wuskell JP, Loew LM, Kohl P. Single-sensor system for spatially resolved, continuous, and multiparametric optical mapping of cardiac tissue. *Heart Rhythm Off J Heart Rhythm Soc*. 2011 Sep;8(9):1482–91.
73. Fast VG. Recording Action Potentials Using Voltage-Sensitive Dyes. In: Dhein PDS, Mohr PDFW, MD MD, editors. *Practical Methods in Cardiovascular Research*. Springer Berlin Heidelberg; 2005. p. 233–55.
74. Baxter WT, Davidenko JM, Loew LM, Wuskell JP, Jalife J. Technical features of a CCD video camera system to record cardiac fluorescence data. *Ann Biomed Eng*. 1997 Aug;25(4):713–25.

75. Vaquero M, Calvo D, Jalife J. Cardiac fibrillation: from ion channels to rotors in the human heart. *Heart Rhythm Off J Heart Rhythm Soc.* 2008 Jun;5(6):872–9.
76. Coates CG, Denvir DJ, McHale NG, Thornbury KD, Hollywood MA. Optimizing low-light microscopy with back-illuminated electron multiplying charge-coupled device: enhanced sensitivity, speed, and resolution. *J Biomed Opt.* 2004 Dec;9(6):1244–52.
77. Daniel M. Bollag, Michael D. Rozycki, Stuart J. Edelstein. *Protein Methods*, 2nd Edition.
78. Mullis KB. The unusual origin of the polymerase chain reaction. *Sci Am.* 1990 Apr;262(4):56–61, 64–5.
79. Valasek MA, Repa JJ. The power of real-time PCR. *Adv Physiol Educ.* 2005 Sep;29(3):151–9.
80. Garibyan L, Avashia N. Polymerase Chain Reaction. *J Invest Dermatol.* 2013 Mar;133(3):e6.
81. Weier HU, Gray JW. A programmable system to perform the polymerase chain reaction. *DNA Mary Ann Liebert Inc.* 1988 Aug;7(6):441–7.
82. Enzoklop. Schematic drawing of the PCR cycle. 2014.
83. VanGuilder HD, Vrana KE, Freeman WM. Twenty-five years of quantitative PCR for gene expression analysis. *BioTechniques.* 2008 Apr;44(5):619–26.
84. alamarBlue® Cell Viability Assay Protocol.
85. Sánchez PL, Fernández-Santos ME, Costanza S, Climent AM, Moscoso I, Gonzalez-Nicolas MA, et al. Acellular human heart matrix: A critical step toward whole heart grafts. *Biomaterials.* 2015 Aug;61:279–89.
86. Blazeski A, Kostecki GM, Tung L. Engineered heart slices for electrophysiological and contractile studies. *Biomaterials.* 2015 Jul;55:119–28.

Appendix 1: Migration and displacement software package

The aim of this software is to obtain confluence graphs over time by processing the image sequence obtained from the time-lapse imaging equipment **Fig. 25**.

The first step is to increase the contrast in the images by subtracting the background and increasing the contrast using ImageJ. Once the image sequence is processed and saved, the Time-lapse analyser can be run. The folder where the original sequence and the processed sequence are selected using the browse option in the red panel. The user can select the wound area and check and choose the intensity values that best segment the cells in that area. It also gives the possibility of analysing the sequence skipping frames in order to obtain faster results. Once the chosen values are appropriate, pressing run the whole sequence starts to be processed with the parameters introduced. The result is shown in real time in the orange panel. The top graph corresponds to the filtered confluence graph and the bottom one to the original one. They are obtained by calculating the area covered by cells over the total wound area using intensity thresholding and morphological operators. The time elapsed from the first frame is obtained from the image information. The user has the possibility of saving the graphs for further plots.

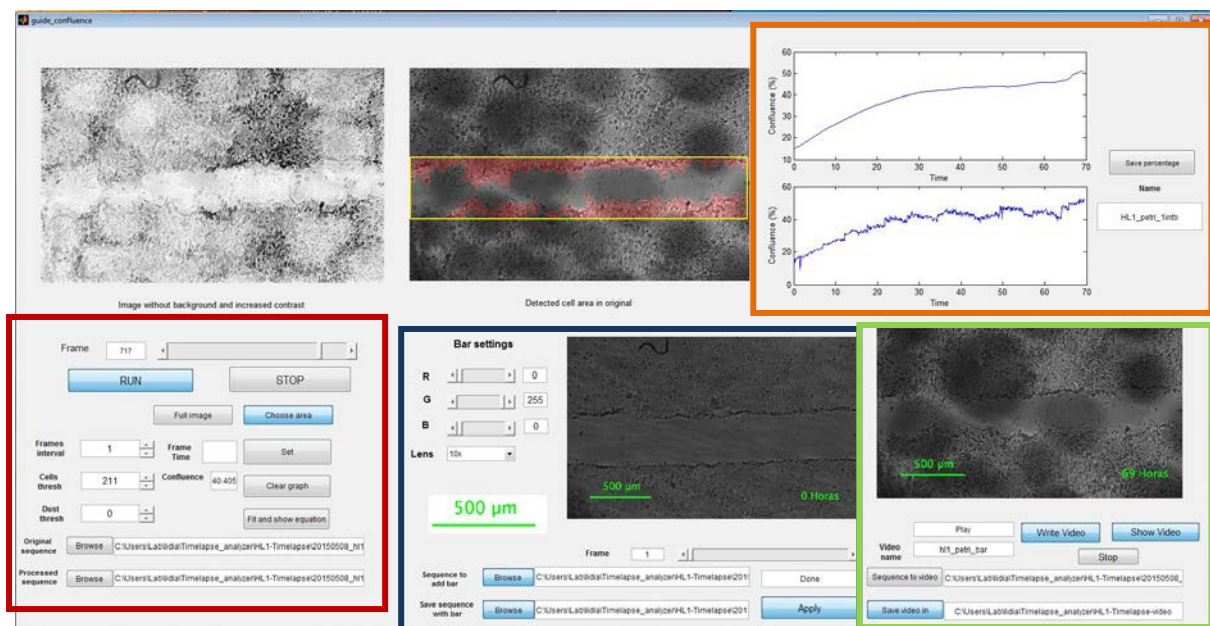


Fig. 25. Time-lapse analyser interface.

The blue panel has the options for adding the time code and the spatial scale to the image sequence. The folder containing the image sequence to which it is desired to add the codes is selected, and the folder where the new image sequence is going to be saved too. The user can choose the bar colour and the objective of the lens used to add the appropriate bar (determined from calibration). Time code is extracted again from the image information.

The green panel creates a time-lapse video from the image sequence introduced. The user selects the folder to which the video is saved and its name, and the video is created at 30 frames per second.

The interface for calculating displacement velocity can be seen in **Fig. 32**. The user introduces the image sequence in which the cell is going to be tracked. By selecting the objective used in the time-lapse equipment and where the cell is in the desired frames, an average value for the displacement velocity is given, calculated from the travelled distance and the time distance between frames.

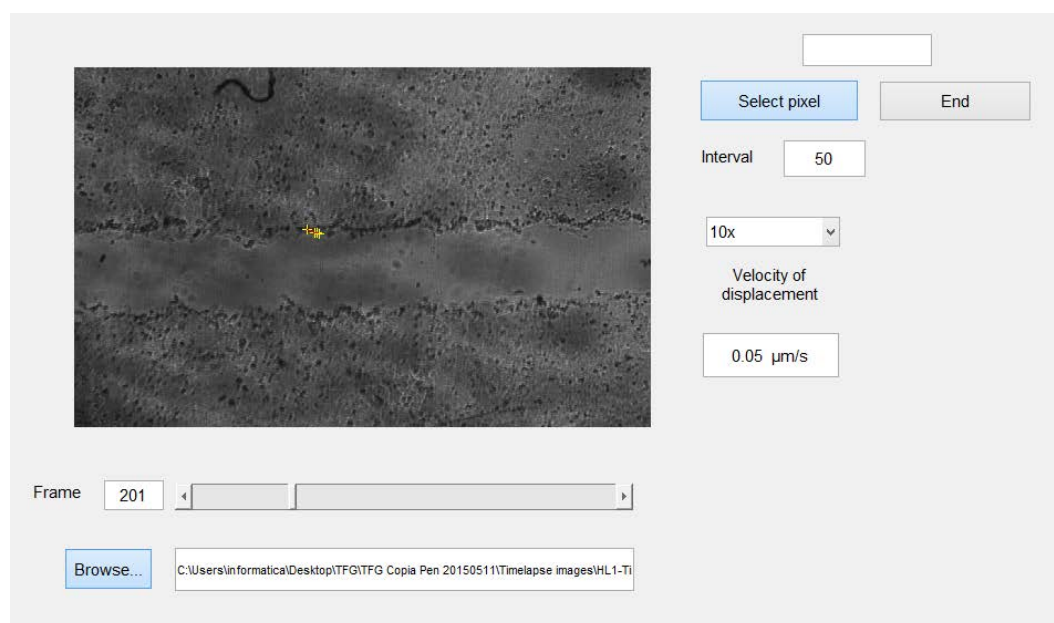


Fig. 32. Displacement velocity software interface.

Appendix 2: Electrophysiology analyser software

The aim of this software is to process recordings from the optical mapping system and give conduction velocity values and isochrones maps to the user (**Fig. 27**).

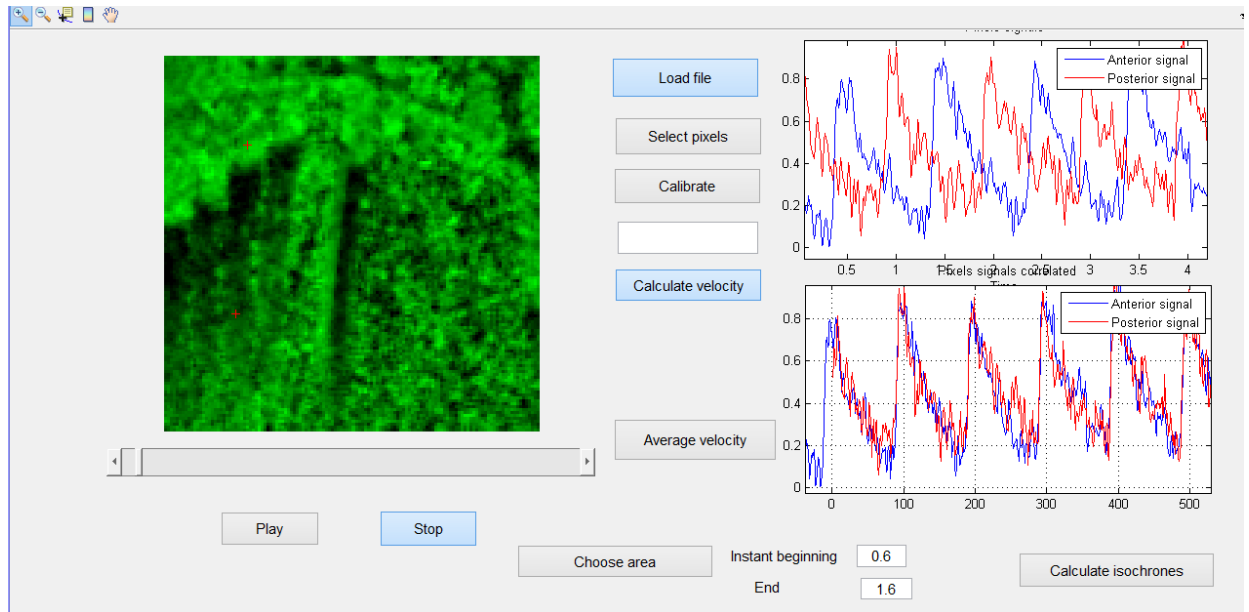


Fig. 27. Electrophysiology analyser Interface.

First, the calibration film (image of a ruler) is loaded. The user selects two pixels whose distance corresponds to one cm to obtain pixel-real distance relationship. Then, the desired film is loaded, and the program performs temporal and spatial filtration before showing the film in the screen. After that, the user can select the two pixels between which the conduction velocity is going to be calculated. The signal of these two pixels is shown in the upper graph for the user to check that these pixels have good action potential signals. By clicking on Calculate velocity button, the signals are correlated and conduction velocity value is given. Correlated signals are shown in the lower graph for the user to check that the process worked as desired and that the value obtained is reliable.

In order to obtain an isochrones map, the user selects an area corresponding to one band showing desired action potential propagation. Then, a beat is introduced by selecting the time instant when it begins and when it ends. The signals in the chosen area and within the chosen time interval are strongly filtered. To calculate the time that the impulse takes to travel from one point to the other, a pixel is taken as reference (in the middle of where the impulse starts propagating). The distance between the instant in which the derivative of the impulse signal is maximum at each pixel with the instance at which the derivative is maximum of the reference pixel is calculated. This is the value that the isochrone map adopts at that point. By showing the isochrones map image with a colour map, the result is the one obtained in **Fig. 29**.

Appendix 3: $2^{-(\Delta\Delta C(T))}$

The $2^{-(\Delta\Delta C(T))}$ method is a common procedure to analyse PCR results. C_t is the value of the amplification cycle in which fluorescence reaches a threshold. The shorter its value, the more fluorescence and the more the gene was expressed. But differences in gene amount or pipetting mistakes may alter the C_t point. That is why housekeeping genes are used. These are genes that do not generally alter their expression.

Thus, the first step in the $2^{-(\Delta\Delta C(T))}$ method is to subtract the C_t value of the gene that is being studied and the C_t value of the housekeeping ($\Delta C(T)$). One of these values is considered as reference (in our case, the Petri sample). Then, the reference $\Delta C(T)$ value is subtracted from the $\Delta C(T)$ values of all samples ($\Delta\Delta C(T)$). The last step is elevating the base two to the $-(\Delta\Delta C(T))$ value. In the reference sample, this value is always close to 1 (depending on primer efficiency), and in the other samples this value represents the relative gene expression with respect to the difference. For example, a $-(\Delta\Delta C(T))$ of 2 means that the studied gene is expressed twice as much as in the reference sample.

In order to confirm that the obtained $-(\Delta\Delta C(T))$ of a sample differs enough with the reference one and to confirm that it is higher or lower expressed, t-test is usually performed. This statistic test takes into account the number of replicates and repetitions and the variance within values for the same sample to determine the probability of making a certain statement.

List of tables and figures

List of Tables

Table 1. Proliferation test.	21
Table 2. Primers used for reverse transcription polymerase chain reaction (RT-PCR).	26
Table 3. Expenses of cell culture.	27
Table 4. Proliferation tests expenditure.	27
Table 5. Migration and displacement tests expenditure.	28
Table 6. Optical mapping tests expenditure.	28
Table 7. Analysis of gene expression tests expenditure.	28
Table 8. Total material and equipment costs.	29
Table 9. Total personnel costs.	29

List of Figures

Fig. 1 Cardiomyocyte structure [13].	3
Fig. 2. Phases of the action potential (A) of a standard cardiomyocyte model and its relation with contraction (B) [19].	5
Fig. 3. Potassium channel, sodium-potassium active pump and sodium channel [20].	6
Fig. 4 Cardiac muscle structure [24].	7
Fig. 5. Cell proliferation.	9
Fig. 6. Patch-clamp technique.	11
Fig. 7 Optical mapping system.	12
Fig. 8. Example of isochrone map and action potential signals obtained using optical mapping technique.	13
Fig. 9 Jablonski diagram of absorbance, non-radiative decay, and fluorescence [58].	13
Fig. 10. Styryl dyes location in the cell membrane.	14
Fig. 11. Emission spectral shift in non-ratiometric calcium indicators.	15
Fig. 12 Polymerase Chain reaction process [82].	18
Fig. 13 Different substrates used: Petri dish (A) and PDMS silicon well (B).	19
Fig. 14 Proliferation assay steps.	21
Fig. 15. Stencil for wound generation.	22
Fig. 16. Lumascope 400 iVue Time-lapse.	22
Fig. 17. Optical mapping of tissue culture.	24
Fig. 18. p35 (A) and silicon well (B) for optical mapping with stimulation electrodes (blue) and impulse propagation direction (purple).	24

Fig. 19. Process for calculating conduction velocity. (1) Calibration. (2) Pixel selection. (3) Correlation of fluorescent signal in time of pixel 1 and pixel 2 (4) Calculate conduction velocity as Spatial distance (cm)/Correlation distance (s).....	25
Fig. 20. HL-1 images at different confluence levels in Petri dishes (A) and in silicon wells (B).	31
Fig. 21. Colorimetric changes produced by alamarBlue® reduction in Petri (P) and silicon wells (S). White is represented by letter B (medium without cells). (+), (~) and (-) correspond to the different initial concentrations indicated in Table 1.	31
Fig. 22. Proliferation in time in both substrates (Petri and Silicon) at different initial concentrations.	32
Fig. 23. Relative reduction with respect to initial concentration over time.	32
Fig. 24. Wound test results in Petri and Silicon.	33
Fig. 25. Time-lapse analyser interface.	34
Fig. 26. Wound area covered with cells in time in both substrates.	34
Fig. 27. Electrophysiology analyser Interface.	35
Fig. 28. Average conduction velocity for each substrate. Differences are statistically significant when $p < 0.05$ (*) (TTest).	36
Fig. 29. Isochrone maps of a significant band in each substrate.	36
Fig. 30. Expression levels of ion channels in HL1 cells grown in silicon versus Petri substrates. SCN5A, CACNA1C and KCNJ2 genes codify for proteins which are subunits of ion channels associated to <i>INa</i> , <i>ICaL</i> and <i>IK1</i> respectively. Differences are statistically significant when $p < 0.05$ (*) (TTest).	37
Fig. 31. Expression levels of connexin genes in HL1 cells grown in silicon versus Petri substrates. GJA5, GJA1, GJA7 genes codify for components of the gap junctions: connexin 40, connexin 43 and connexin 45 respectively. Differences are statistically significant when $p < 0.05$ (*) (TTest).	37
Fig. 32. Displacement velocity software interface.	50